A Genetic Program Mediates Cold-warming Response and Promotes Stress-induced Phenoptosis in *C. elegans*

Wei Jiang[1, 2]†, Yuehua Wei[1]†, Yong Long[1, 3]†, Arthur Owen[4], Bingying Wang[1], Xuebing Wu[5], Shuo Luo[5], Yongjun Dang[2], Dengke K. Ma[1]*

[1]Cardiovascular Research Institute and Department of Physiology, University of California San Francisco, San Francisco, CA 94158

[2]Key Laboratory of Molecular Medicine, Ministry of Education and Department of Biochemistry and Molecular Biology, School of Basic Medical Sciences, Shanghai Medical College, Fudan University, Shanghai, 200032, China

[3]State Key Laboratory of Freshwater Ecology and Biotechnology, Institute of Hydrobiology, Chinese Academy of Sciences, Wuhan 430072, China

[4]Department of Molecular Cell Biology, University of California Berkeley, Berkeley, CA 94720

[5]Department of Biology, Massachusetts Institute of Technology, 9 Cambridge Center, Cambridge, MA 02142

†These authors contributed equally to this work

*For Correspondence: Dengke.Ma@ucsf.edu

Abstract

How multicellular organisms respond to and are impacted by severe hypothermic stress is largely unknown. From *C. elegans* screens for mutants abnormally responding to cold-warming stimuli, we identify a molecular genetic pathway comprising ISY-1, a conserved uncharacterized protein, and ZIP-10, a bZIP-type transcription factor. ISY-1 gatekeeps the ZIP-10 transcriptional program by regulating the microRNA *mir-60*. Downstream of ISY-1 and *mir-60*, *zip-10* levels rapidly and specifically increase upon transient cold-warming response. Prolonged *zip-10* up-regulation induces several protease-encoding genes and promotes stress-induced organismic death, or phenoptosis, of *C. elegans*. *zip-10* deficiency confers enhanced resistance to prolonged cold-warming stress, more prominently in adults than larvae. We conclude that the ZIP-10 genetic program mediates cold-warming response and may have evolved to promote wild-population kin selection under resource-limiting and thermal stress conditions.

Introduction

Temperature shifts pervasively affect numerous biological processes in all organisms. Heat shock stimuli activate expression of many heat-shock inducible genes through the sigma-32 factor and the evolutionarily conserved transcription factor HSF (Heat Shock Factor) in bacteria and eukaryotes, respectively (Gomez-Pastor et al., 2017; Yura et al., 1993). Coordinated expression of heat shock-induced chaperone proteins facilitates cellular proteostasis and adaptation to temperature upshift (Mahat et

al., 2016; Solís et al., 2016). In contrast to heat shock response, how organisms respond to cold shock is still largely unknown (Al-Fageeh and Smales, 2006; Choi et al., 2012; Yenari and Han, 2012; Zhu, 2016). Although extensive RNA expression profiling studies have identified many protein-coding genes and non-coding RNAs that are regulated by cold shock via both transcriptional and post-transcriptional mechanisms (Al-Fageeh and Smales, 2006; Giuliodori et al., 2010; Kandror et al., 2004; Zhou et al., 2017), master regulators of cold shock response and cold-regulated genes (counterparts of HSF) have long been elusive and mechanisms of cold shock response in multicellular organisms remain poorly characterized.

At the organismic level, warm-blooded mammals normally keep body temperature at about 37^{o}C and initiate multiple homeostatic mechanisms to maintain body temperature upon exposure to hypothermia (Bautista, 2015; Morrison, 2016; Tansey and Johnson, 2015; Vriens et al., 2014). In humans, therapeutic hypothermia (32-34^{o}C) has been widely used to treat ischemic disorders and proposed to activate multifaceted cellular programs to protect against ischemic damages (Choi et al., 2012; Polderman, 2009; Yenari and Han, 2012). By contrast, cold-blooded animals including most invertebrates experience varying body temperature depending on the environment, but can nonetheless elicit stereotypic behavioral, physiological and transcriptional response to chronic hypothermia or transient cold shock (Al-Fageeh and Smales, 2006; Garrity et al., 2010). Like many other types of stress, prolonged severe hypothermia can lead to the death of organisms, in most cases likely because of failure in adapting to the stress, or alternatively through stress-induced phenoptosis, namely genetically programed organismic death (Longo et al., 2005; Skulachev, 1999, 2002).

Although phenoptosis has been phenotypically documented in many cases, its evolutionary significance and genetic mechanisms remain unclear and debated (Longo et al., 2005; Sapolsky, 2004).

We previously discovered a *C. elegans* genetic pathway that maintains cell membrane fluidity by regulating lipid desaturation in response to moderate hypothermia (10-15^{o}C) (Fan and Evans, 2015; Ma et al., 2015). Expression of the gene *fat-7*, which encodes a lipid desaturase, is transcriptionally induced by 10-15^{o}C but not by more severe hypothermia (i.e. cold shock at 0-4^{o}C), which impairs *C. elegans* reproduction and growth, and elicits distinct physiological and behavioral responses (Garrity et al., 2010; Lyons et al., 1975; Ma et al., 2015; Murray et al., 2007). However, as severe hypothermia arrests most of cell biological processes, strong transcriptional responses to cold shock e.g. 0-4^{o}C likely only manifest during the organismic recovery to normal ambient temperature. We thus hypothesize that a genetic pathway differing from that operating under moderate hypothermia exposure controls the transcriptional response to severe hypothermia/cold shock followed by warming in *C. elegans*.

In this work, we performed transcriptome profiling to first identify genes that are regulated by exposure to cold shock followed by recovery at normal temperature. We then used GFP-based transcriptional reporters in large-scale forward genetic screens to identify a genetic pathway consisting of *isy-1* and *zip-10*, the latter of which responds to cold-warming (CW) and mediates transcriptional responses to CW. Unexpectedly, we found strong *zip-10* induction promotes organismal death while deficiency of *zip-10* confers resistance to prolonged CW stress, more prominently in adults than young larvae. We propose that CW activates a ZIP-10 dependent genetic program favoring *C.*

elegans phenoptosis and postulate that such programmed organismic death may have evolved to promote wild-population kin selection under thermal stress conditions.

Results

To identify new mechanisms of *C. elegans* response to severe hypothermia, we performed RNA sequencing (RNA-seq) of wild-type *C. elegans* populations after 2-hr exposure to 4^{o}C cold shock followed by recovery at 20^{o}C for 1 hr. We used such CW conditions in an attempt to identify genes that specifically and rapidly respond to CW rather than those that respond to general organismic deterioration after long cold exposure. After differential expression analyses of triplicate samples, we identified 604 genes that are significantly up- or down-regulated by such CW conditions (Figure 1-source data 1, Figure 1A and Figure 1-figure supplement 1A). Gene ontology analysis indicated that the CW-regulated genes are involved in biological processes including lipid metabolisms, autophagy, proteostasis and cell signaling (Figure 1-figure supplement 1B). We generated transgenic *C. elegans* strains in which *GFP* is driven by promoters of the top-ranked CW-inducible genes. In this work, we focus on *asp-17* as a robust CW-inducible reporter gene owing to its low baseline expression level and high-fold induction by CW, features that permitted facile isolation of full-penetrance mutants after random mutagenesis (see below) with both abnormal *asp-17p::GFP* expression and altered organismic tolerance to prolonged cold stress.

C. elegans asp-17 encodes an aspartyl-like protease with unknown molecular functions. Like other CW-inducible genes, *asp-17* up-regulation is more prominently

induced by severe than moderate hypothermia followed by recovery from cold shock (Figures 1B and 1C). Among the aspartyl-like protease family members, we found that only *asp-17* was robustly and specifically induced by CW (Figure 1D). The up-regulation of endogenous *asp-17* by CW can be recapitulated by an integrated GFP reporter driven by the endogenous *asp-17* promoter, indicating transcriptional regulation of *asp-17* by CW (Figure 2-Figure supplement 1A). We varied CW treatment conditions and found that the induction of *asp-17* strictly required the warming phase after cold shock (Figure 1E). However, heat shock at 32^{o}C did not increase *asp-17* expression (Figure 1E), consistent with previous large-scale transcriptome profiling studies in *C. elegans* (Brunquell et al., 2016). Single-molecule fluorescent in-situ hybridization (smFISH) identified the CW-induced *asp-17* predominantly in intestinal cells (Figure 1F). Since CW activates numerous other genes in addition to *asp-17*, we sought to use *asp-17p::GFP* as a robust readout reporter to identify the upstream genetic pathway and transcriptional regulators that control *asp-17* induction by CW.

We performed a forward genetic screen using EMS-induced random mutagenesis of a parental strain carrying a genome-integrated *asp-17p::GFP* reporter and isolated over 30 mutants with constitutive *asp-17p::GFP* expression in the absence of CW (Figure 2-figure supplement 1B and 1C). We molecularly cloned one mutant *dma50* that exhibited fully penetrant and constitutively strong expression of *asp-17p*::*GFP* (Figure 2A,B and Figure 2-figure supplement 1D-1F). Compared with wild type, *dma50* strongly up-regulated *asp-17*::*GFP* in the intestine (Figure 2B). By single nucleotide polymorphism-based linkage analysis of the intestinal *asp-17p*::GFP phenotype, we mapped *dma50* to a genetic interval on Chromosome V and used whole-

genome sequencing to identify candidate causal gene mutations (Figure 2-figure supplement 1D,E). Based on phenocopying by feeding RNAi and transformation rescue of the *asp-17p*::GFP phenotype, *dma50* defines a previously uncharacterized *C. elegans* gene *isy-1* (Figures 2A-2F and Figure 2-figure supplement 1F). *isy-1* (*I*nteractor of *SY*F1 in yeast) encodes a protein with strong sequence similarity to an evolutionarily highly conserved family of RNA-binding proteins in eukaryotes (Figure 2A and Figure 2-figure supplement 2A-2C) (Dix et al., 1999; Du et al., 2015).

dma50 caused substitution of a negatively charged glutamate, which is completely conserved in the ISY protein family, to a positively charged lysine in the predicted coiled-coil region of *C. elegans* ISY-1 (Figure 2A). An *isy-1p::isy-1::GFP* translational reporter indicated a rather ubiquitous distribution of ISY-1::GFP in many tissues including intestinal nuclei (Figure 2C). The strong intestinal *asp-17p*::GFP expression caused by *dma50* was fully rescued by transgenic expression of wild-type *isy-1*(+), single-copy integration of a *mCherry*-tagged *isy-1(+)* allele, or *isy-1*(+) expression driven by the intestine-specific *ges-1* promoter (Figures 2E and 2F). In addition, the *ges-1*-driven transgenic expression of sense plus antisense *isy-1* RNAi fully recapitulated the *dma50* phenotype (Figure 2D). Endogenous expression of *asp-17* was also drastically up-regulated in *isy-1* mutants (Figure 2-Figure supplement 2D). Thus, these results identify *isy-1* as a causal cell-autonomous regulator of *asp-17*.

Human ISY1 is critical for certain microRNA processing while yeast ISY1 is a likely component of the spliceosome (Dix et al., 1999; Du et al., 2015; Galej et al., 2016). We found that CW-induced *asp-17* up-regulation was further enhanced in *isy-1* mutants compared with wild type (Figure 3A), suggesting that ISY-1 normally restricts

transcriptional activity of *asp-17*. To determine the mechanism by which ISY-1 regulates transcription of *asp-17*, we sought to identify transcription factors (TF) that meet two criteria: a), its mRNA or protein products are altered in *isy-1* mutants, and b), it is genetically epistatic to *isy-1*, i.e. its loss-of-function (LOF) can suppress *isy-1* LOF (thus also likely required for *asp-17* induction by CW). We performed RNA-seq from triplicate samples of wild-type hermaphrodites and *isy-1* mutants, from which we analyzed differentially expressed TF-encoding genes in *isy-1* mutants and found that a bZIP-type transcription factor-encoding gene *zip-10* met both criteria (Figure 3B, Figure 3-source data 1). *zip-10* mRNA was drastically up-regulated in *isy-1* mutants, whereas levels of closely related bZIP family genes, such as *zip-11*, were unaffected (Figure 3C). Importantly, genetic deletion of *zip-10* completely abrogated the ability of *isy-1* RNAi to activate *asp-17p::GFP* (Figure 3D). These results indicate that ISY-1 regulates *asp-17* by controlling the level of *zip-10* mRNAs.

Next, we examined how the ISY-1/ZIP-10/ASP-17 pathway is regulated by CW. CW did not apparently alter levels of endogenous *isy-1* mRNAs or mCherry-tagged ISY-1 proteins under the endogenous *isy-1* promoter (Figure 2-Figure supplement 2D and 2E). By contrast, we found that CW induced drastic up-regulation of ZIP-10 proteins from a tagged *zip-10p::zip-10::EGFP::FLAG* allele in an integrated transgenic strain (Figure 3E). Although EGFP fluorescence was invisible in animals carrying such transgenes (likely because it is sandwiched by *zip-10* and FLAG), the striking induction of ZIP-10::EGFP::FLAG was completely blocked by RNAi against *zip-10* or *GFP*, confirming the transgene specificity (Figure 3F). The baseline level of ZIP-10::EGFP::FLAG was close to the detection limit of Western blot under normal

conditions, but nonetheless is strongly up-regulated upon RNAi against *isy-1* (Figure 3F). Similar to that of *asp-17*, the induction of *zip-10p::zip-10::EGFP::FLAG* strictly required the warming phase of CW and occurred rapidly but transiently after warming during CW (Figure 3G). CW strongly up-regulated *asp-17* expression in both wild type and *isy-1* mutants, which exhibited abnormally high *zip-10* mRNA levels (Figure 3H). Furthermore, *zip-10* deletion completely abrogated the up-regulation of *asp-17* levels by CW (Figure 3I). We also examined the ZIP-10 dependency of other CW-inducible genes identified by RNA-seq and found that at least *cpr-3* also required ZIP-10, but other CW-inducible genes including *srr-6* and *F53A9.1*, did not (Figure 3I). These results demonstrate that ISY-1 suppresses *asp-17* by decreasing *zip-10* levels whereas CW up-regulates ZIP-10 protein abundance to promote *asp-17* expression.

How is *zip-10* regulated by ISY-1 and CW? Loss of ISY-1 function affected neither general intron splicing based on an intronic GFP reporter assay, nor specific splicing of *zip-10*, although both CW and *isy-1* mutations strongly up-regulated *zip-10* mRNA levels (Figure 3-Figure supplement 1A-1E). We constructed a GFP transcriptional reporter driven by the endogenous *zip-10* promoter and found it was markedly up-regulated by *isy-1* RNAi (Figure 3-Figure supplement 2A). While non-thermal stresses such as hypoxia and starvation did not increase ZIP-10 levels, CW drastically increased abundance of ZIP-10 in both cytosol and nucleus without affecting abundance of other house-keeping proteins, including HSP90, tubulin and histone H3 (Figure 3-Figure supplement 2B and 2C). CW up-regulation of ZIP-10 required warming and was enhanced by more prolonged cold shock (Figure 3-Figure supplement 2D). Since CW can markedly increase *zip-10* mRNA levels but to a lesser extent than the

183 *isy-1* mutation (Figure 3-Figure supplement 1D and 1E), we tested whether ZIP-10
184 proteins might be regulated by CW through translational control and mRNA stability.
185 RNAi against genes encoding eIF5 and a component of the Ccr4-Not complex did not
186 apparently alter ZIP-10 levels (Figure 3-Figure supplement 2E). Together, these results
187 indicate that CW and ISY-1 regulate *zip-10* primarily at the transcriptional level.

188 Human ISY1 facilitates the processing of primary transcripts encoding certain
189 families of microRNAs (Du et al., 2015). Both *zip-10* and *asp-17* are up-regulated in a
190 mutant *C. elegans* strain deficient in the microRNA *mir-60* (Kato et al., 2016). We thus
191 tested whether *mir-60* mediates the regulation of *zip-10* by ISY-1. Immunoprecipitation
192 of mCherry-tagged ISY-1 followed by quantitative PCR (QPCR) revealed specific
193 binding of primary transcripts encoding *mir-60* as well as a protein-coding gene *cebp-1*
194 (Figure 4A-4C). Although neither *isy-1* nor *mir-60* levels were affected by CW, we found
195 CW slightly increased *mir-60* binding to ISY-1, perhaps as a feedback mechanism to
196 limit over-activation of *zip-10*-dependent genes after CW treatment (Figure 4B).
197 Importantly, mature *mir-60* levels were drastically decreased in *isy-1* mutants while loss
198 of *mir-60* led to up-regulation of *zip-10* and *zip-10*-dependent subset of CW-inducible
199 genes, including *asp-17* and *cpr-3,* but not many other CW-inducible genes (Figure 4D,
200 4E and Figure 4-figure supplement 1). The 3' untranslated region (Utr) of *zip-10*
201 appeared not to be regulated by CW or *isy-1* RNAi (Figure 4F). However, *isy-1* RNAi
202 caused an abnormally high baseline level of ZIP-10 in the absence of CW and enabled
203 further heightened ZIP-10 up-regulation in response to CW, followed by its down-
204 regulation over an extended period of warming (Figure 4G). These results indicate that
205 CW regulates transcription of *zip-10* (and thereby that of *asp-17*), while ISY-1 controls

206 expression of *zip-10* via *mir-60*, likely through microRNA processing and regulation of
207 additional upstream transcriptional *zip-10* regulators that respond to CW.

208 We compared the genes differentially regulated by CW and those by *isy-*
209 *1(dma50)* mutants and found 246 genes, including the two ZIP-10 dependent targets
210 *asp-17* and *cpr-3*, that are commonly regulated by both conditions (Figure 5A, Figure 5-
211 source data 1). Global transcriptome changes between these two conditions are also
212 significantly correlated (Figure 5B) (correlation coefficient *R* as 0.54, significance *P*
213 value as 0). We used the bioinformatics tool MEME (Bailey et al., 2009) to identify
214 motifs present in the promoters (~600 bp upstream of transcription start sites) of the
215 commonly regulated gene subset and identified a single enriched motif characterized by
216 AT-rich sequences (Figure 5C). The gene most enriched with this motif is *asp-17*, the
217 promoter of which contains 16 such motifs (Figure 5C). ZIP-10 is a bZIP-type
218 transcription factor predicted to contain N-terminal low sequence-complexity domains
219 and a C-terminal DNA-binding and glutamine-rich transactivation domain (Figure 3-
220 Figure supplement 2F-2H). To test whether the *asp-17* promoter with the identified AT-
221 rich motifs can be bound directly by ZIP-10, we performed chromatin
222 immunoprecipitation (ChIP) experiments and detected *asp-17* promoter sequences in
223 the FLAG-tagged ZIP-10 chromatin complex only under CW conditions (Figure 5D).
224 These results indicate that ZIP-10 directly binds to and activates the *asp-17* promoter in
225 the genetic program regulated by ISY-1 and CW.

226 The striking regulation of *zip-10* and *asp-17* by CW and ISY-1 prompted us to
227 examine the organismic phenotype of various mutants upon prolonged CW stress. A
228 majority of wild-type *C. elegans* adults died upon prolonged CW stress (e.g. 2-4^{o}C for

over 24 hrs) (Ohta et al., 2014). We found that *asp-17* or *zip-10* loss-of-function mutants exhibited markedly higher survival rates than wild type under the same prolonged CW stress condition (Figure 5E). Consistent with a role of wild-type *zip-10* in promoting organismic death, inducible *zip-10* over-expression by mild transient heat shock, mediated by the *hsp-16* promoter, promoted animal death even in the absence of CW (Figure 5F). By contrast, other ectopically induced *zip* genes including *zip-11* and *zip-2* did not affect animal death, while a mutation specifically disrupting the glutamine-rich transactivation domain of ZIP-10 abolished the death-promoting effect (Figures 5F and Figure 3-Figure supplement 2H). Although *zip-10* is genetically epistatic to *isy-1* in the regulation of *asp-17*, we found that *isy-1* mutants are also markedly resistant to prolonged cold stress. This paradox was resolved after we observed that many downstream target genes of the stress-coping transcription factors HIF-1, HSF-1 and DAF-16 are up-regulated in *isy-1* mutants, and LOF of at least *daf-16* could partly suppress cold tolerance by *isy-1* RNAi (Figures 5G and 5H). Since ISY-1 regulates *zip-10* via *mir-60* (Figure 4) supporting a role of ISY-1 in specific microRNA processing (Du et al., 2015), we performed small RNA library sequencing of wild type animals and *isy-1* mutants and identified specific members of microRNAs that were differentially regulated, including *mir-60* and additional microRNAs predicted to target stress-coping TFs (Figure 5-Figure supplement 1A-1F). Thus, *isy-1* mutants likely exhibit pleiotropic phenotypes caused by abnormal activation of multiple TFs in addition to ZIP-10. In contrast to ZIP-10 dependent genes (*asp-17* and *cpr-3*), the HIF-1/HSF-1/DAF-16 target genes were not apparently induced by CW (Figure 1-source data 1). Furthermore, unlike HSF-1 or DAF-16 that are induced by other types of stress stimuli, ZIP-10 is more

252 strongly induced by CW in adults than in larvae (Figure 5-figure supplement 2C),
253 suggesting phenoptosis-promoting effects of *zip-10* for adults more specifically. Indeed,
254 the phenotypic difference in cold tolerance between wild type animals and *zip-10*
255 mutants manifested more prominently in developmentally more mature-stage and older
256 animals (Figure 5-figure supplement 2D). These results indicate that CW specifically
257 activates a ZIP-10-driven and developmental stage-modulated transcriptional genetic
258 program to promote the organismic death, or phenoptosis, of *C. elegans* (Figure 5I).

259

260 **Discussion**

261 From a genetic screen for *C. elegans* mutants with altered transcriptional
262 response to CW, we identified *isy-1* and subsequently discovered the CW and ISY-1-
263 regulated transcription factor ZIP-10 as a key mediator of the transcriptional response to
264 CW. A thermal stress-responding TF might be expected to promote adaptation of
265 animals towards the stressor, causing its LOF mutants to be sensitive to the stress.
266 Unexpectedly, we found *zip-10* mutants are markedly resistant to prolonged cold stress.
267 However, unlike other stress-responding TFs that activate genes largely beneficial for
268 physiological homeostasis and thus animal health under stress conditions (Baird et al.,
269 2014; Dempersmier et al., 2015; Hwang and Lee, 2011; Kandror et al., 2004; Kumsta et
270 al., 2017; Landis and Murphy, 2010), identified transcriptional targets of ZIP-10 include
271 at least two Cathepsin-type proteases, CPR-3 and ASP-17 (Figure 4E). In contrast to
272 aspartyl-type proteases which are largely unknown in cellular functions, caspase-type
273 proteases are well-known apoptotic cell death executioners while CPR-4, a Cathepsin

CPR-3 paralogue, has been shown to inhibit cell deaths in *C. elegans* (Metzstein et al., 1998; Peng et al., 2017; Peter, 2011). Ectopic expression of *zip-10* and its targets promotes organismic deaths, in contrast to the effect of *zip-10* or *asp-17* deficiency on cold tolerance (Figure 5E and 5F). As duration of cold shock affects levels of ZIP-10 and transient CW does not trigger phenoptosis, the pro-death role of the *zip-10* genetic program likely depends on multiple factors, including the duration and severity of cold exposure. Notably, apoptotic cell death-promoting effects have also been described for specific members of mammalian bZIP TFs (Chüeh et al., 2017; Hartman et al., 2004; Ritchie et al., 2009). The specific and robust induction of ZIP-10 by CW, the opposing cold-tolerance phenotypes caused by *zip-10* loss-of-function and gain-of-function genetic manipulations, as well as the pro-death roles of ZIP-10 targets support the notion that the *zip-10* pathway is activated by severe CW to promote phenoptosis.

How do ISY-1 and CW regulate the *zip-10* pathway? We found that the *zip-10* promoter activity responds to the loss of ISY-1, which normally maintains *mir-60* levels and thereby regulates *zip-10* transcription likely through the processing of small RNAs. Severe cold stress also leads to accumulation of another class of small RNA risiRNA, which is important for maintaining rRNA homeostasis (Zhou et al., 2017). Whether ISY-1 might also affect risiRNA processing remains to be characterized. Constitutive up-regulation of ZIP-10 targets in *isy-1* mutants and the lack of evidence for regulation of ISY-1 by CW supports ISY-1 as a gate-keeper for the ZIP-10-driven transcriptional response to CW (Figure 5I). Regulation of *zip-10* is primarily transcriptional based on evidence we present in this study; further studies are required to discern to what extent *mir-60* might directly act at the *zip-10* locus or more indirectly impact the transcription of

297 *zip-10*, e.g. by post-transcriptionally inhibiting translation of a transcriptional activator.
298 Up-regulation of the activity of the *zip-10* promoter by CW indicates that additional cold-
299 responding sensors and effectors upstream of ZIP-10 remain to be identified, by
300 signaling mechanisms perhaps similar to the well-characterized cold-responding
301 pathways found in other organisms (Dempersmier et al., 2015; Kandror et al., 2004;
302 Zhu, 2016). Precisely how *zip-10* is regulated by CW in coordination with ISY-1 to
303 promote *C. elegans* death under prolonged CW stress awaits further investigation.

304 The roles of ZIP-10 and a dedicated genetic program in promoting organismic
305 death are surprising but would make sense in light of the evolutionary kin selection
306 theory. Kin selection refers to the evolutionary process promoting the reproductive
307 success of an organism's kin despite a cost to the organism's own reproduction
308 (Hamilton, 1963; Smith, 1964). Dedicated genetic programs may have evolved to
309 promote kin selection at the population level. Although the concept and potential
310 mechanisms of programed organismic death, or phenoptosis, are debated, examples of
311 kin selection and stress-induced organismic deterioration have been widely documented
312 in many organisms (Longo et al., 2005; Sapolsky, 2004; Skulachev, 1999, 2002).

313 Laboratory conditions for hermaphroditic *C. elegans* clearly no longer exert
314 selection pressure for genetic programs underlying phenoptosis or kin selection.
315 However, our mathematic modeling of an exemplar situation of population growth for
316 wild-type and *zip-10* deficient animals under food-limiting and CW stress conditions
317 supports the phenoptosis or kin selection hypothesis for the *zip-10* pathway (Figure 5-
318 Figure supplement 2A and 2B). Experimentally, we found that both the CW-induced *zip-*
319 *10* expression and the death-promoting effect of ZIP-10 occurred more prominently in

older adults than in larvae (Figure 5-Figure supplement 2C and 2D). Extending from the kin selection theory, we postulate that the evolutionary advantage of programmed organismic death might manifest in the wild, where resources for growth and reproduction are limited and environments can change drastically. As such, the selective death of adult animals would benefit young and reproductively more privileged populations to facilitate the spreading of genes by young populations under resource-limiting and high-stress conditions. Our work provides an unprecedented example of stress-induced phenoptosis in *C. elegans* and identify a specific transcription factor in a genetic program that likely evolved to promote kin selection during animal evolution. These findings therefore bear broad implications for understanding thermal stress response, programmed organismic death (phenoptosis) and evolutionary biology.

Materials and Methods

C. elegans strains and genetic manipulations

C. elegans strains were maintained with standard procedures unless otherwise specified. The N2 Bristol strain was used as the reference wild type, and the polymorphic Hawaiian strain CB4856 was used for genetic linkage mapping and SNP analysis (Brenner, 1974; Davis et al., 2005). Forward genetic screen for constitutive *asp-17p::GFP* reporter-activating mutants after ethyl methanesulfonate (EMS)-induced random mutagenesis was performed as described previously (Ma et al., 2012, 2015). Single-copy integration of *isy-1p::isy-1::mCherry* transgene was generated using the MosSCI method (Frøkjaer-Jensen et al., 2008). To generate *asp-17* null alleles in *C.*

342 *elegans,* we used CRISPR-Cas9 to induce double stranded breaks and subsequent
343 non-homologous end joining caused a deletion of *asp-17*. Feeding RNAi was performed
344 as previously described (Kamath and Ahringer, 2003). Transgenic strains were
345 generated by germline transformation as described (Mello et al., 1991). Transgenic
346 constructs were co-injected (at 10 - 50 ng/µl) with dominant *unc-54p*::mCherry or *rol-6*
347 markers, and stable extrachromosomal lines of mCherry+ or roller animals were
348 established. Genotypes of strains used are as follows: *daf-16(mu86) I, mir-60(n4947) II*;
349 *isy-1(dma50) V, zip-10(ok3462) V, asp-17(dma99) V, dmaIs10[asp-17p::GFP; unc-*
350 *54p::mCherry] X, dmaIs21[zip-10p::GFP; unc-54p::mCherry]; wgIs634[zip-10p::zip-*
351 *10::EGFP::FLAG + unc-119(+)], oxTi302 [eft-3p::mCherry::tbb-2 3'UTR + Cbr-unc-*
352 *119(+)], dmaSi1[isy-1p::isy-1::mCherry, unc-119(+)], dmaEx95[ges-1p::isy-1(+); rol-*
353 *6(+)], dmaEx99[isy-1 genomic DNA (2ng/ul); rol-6(+)], nEx102[ges-1p::isy-1(+); rol-*
354 *6(+)], nEx103[ges-1p::isy-1(+); rol-6(+)], dmaEx104[ges-1p::mCherry::3utr(zip-10), rol-*
355 *6(+)], dmaEx123[hsp-16p::zip-10; rol-6(+)], dmaEx124[hsp-16p::zip-10; rol-6(+)],*
356 *dmaEx131[zip-10p::GFP; unc-54p::mCherry].*

357

358 Sample and library preparation for RNA sequencing

359 Control N2 animals and the *isy-1* mutants were maintained at 20^{o}C. For cold stress, N2
360 animals were exposed to 4^{o}C for 2 hrs followed by 1 hr recovery at 20^{o}C. Upon sample
361 collection, the animals were washed down from NGM plates using M9 solution and
362 subjected to RNA extraction using the RNeasy Mini Kit from Qiagen. 1 µg total RNA from
363 each sample was used for sequencing library construction. Each treatment included 3

biological replicates. The NEBNext® rRNA Depletion Kit was used for rRNA depletion. After rRNA depletion, the Agencourt RNAClean XP Beads from Beckman Coulter were used for RNA purification. Then, the NEBNext® Ultra™ Directional RNA Library Prep Kit for Illumina® was used for RNA fragmentation, first strand and second strand cDNA synthesis and double-stranded cDNA end repair. Double strand cDNAs were purified using the Agencourt AMPure XP from Beckman Coulter and ligated to adaptors of the NEBNext Multiplex Oligos for Illumina. Finally, the Q5 Hot Start HiFi PCR Master Mix was used for PCR enrichment of the adaptor-ligated DNA. The concentration and quality of the constructed sequencing libraries were measured by using the Agilent High Sensitivity DNA Kit and a Bioanalyzer 2100 from Agilent Technologies. The libraries were submitted to 100 bp paired-end high throughput sequencing using Hiseq-3000 by the Center for Advanced Technology (CAT) of the University of California, San Francisco.

RNA-seq data analysis was performed using a super computer system equipped with multiple processors. The raw reads were trimmed and filtered by the prinseq-lite software (0.20.4) (Schmieder and Edwards, 2011). Reads longer than 30 bp and with a minimum quality score higher than 15 were kept and used for subsequent analyses. The filtered left and right read sets were compared by the Pairfq script to separate paired and single reads. The clean reads were mapped to the *C. elegans* genome sequence using Hisat2 (2.0.5)(Kim et al., 2015) with default parameters. The number of mapped reads were counted by featureCounts from the Subread package (1.5.0) (Liao et al., 2014). Differential gene expression analysis was performed using the DESeq2 package (Love et al., 2014). Adjusted P-value ≤ 0.05 was used as the threshold to identify the differentially expressed genes. Gene ontology and KEGG pathway enrichment analyses

for the differentially expressed genes were conducted using the Cytoscape plugins BiNGO (Maere et al., 2005) and ClueGO (Bindea et al., 2009), respectively. Plots for the mapped reads were generated by IGVtools (Thorvaldsdóttir et al., 2013).

Quantitative RT-PCR

50 µl pellet animals were resuspended in 250 µl lysis buffer of Quick-RNA MiniPrep kit (Zymo Research, R1055) then lysed by TissueRuptor (Motor unit “8” for 1 min). Total RNA was extracted following the instruction (Zymo Research, R1055). 2 µg RNA/sample was reverse transcribed into cDNA (BioTools, B24408). Real-time PCR was performed by using Roche LightCycler®96 (Roche, 05815916001) system and SYBR Green (Thermo Fisher Scientific, FERK1081) as a dsDNA-specific binding dye. qRT-PCR condition was set to 95°C for denaturation, followed by 45 cycles of 10s at 95°C, 10s at 60°C, and 20s at 72°C. Melting curve analysis was performed after the final cycle to examine the specificity of primers in each reaction. Relative mRNA was calculated by ΔΔCT method and normalized to actin. Primers for qRT-PCR: *asp-17* (Forward, ATGTTCCGCTGACTGCGAAG; Reverse, TTTCATTCATTTCATCCCAC), *F53A9.1*, Forward, ACTACGGAAACGGAGGATAC; Reverse, TGGCCGTGATGATGATGATG), *srr-6* (Forward, CTCCAAGTCCTGAAGTCGTG; Reverse, GTAGGGATGGATTGAACTCG), *isy-1* (Forward, AGATGCTGAGCGATTCAGAC; Reverse, CTTTCGATAGTCCGTACCAC), *zip-10* (Forward, TCGAGATGCTCTTCAACTG; Reverse, CTAACTGCTTGCCGGAG), *cpr-3* (Forward, GTAGTGGAGCAGTAACAGGTG; Reverse,

409 CAGTTTGAATTTCGGTGACGG), *act-3* (Forward, TCCATCATGAAGTGCGACAT;
410 Reverse, TAGATCCTCCGATCCAGACG).

411

412 Sample preparation and Western blot of proteins

413 Transgenic (*isy-1p::isy-1::mCherry* and *zip-10p::zip-10::EGFP::FLAG*) animals
414 were cold shocked (4^{o}C) for 0, 1, 2 or 4 hrs, followed by recovery at 25^{o}C for 1 h. Animals
415 were harvested and washed 3 times with M9 and 20 µl pellet animals were lysed directly
416 in Laemmli Sample Buffer and used for Western blot analysis. Proteins were resolved by
417 15% SDS-PAGE (Bio-Rad, 4561084) and transferred to a nitrocellulose membrane (Bio-
418 Rad, 1620167). Proteins were detected using antibodies against Flag (Sigma, F3165),
419 mCherry (M11217, Life Technologies), Tubulin (Sigma, T5168), H3 (Abcam, ab1791) or
420 HSP90 (Proteintech, 13171-1-AP).

421 For subcellular fractionation, 50 µl pellet animals were resuspended in 150 µl 1 X
422 cell lysis buffer (Cell Signaling Technology, 9803S) with protease inhibitor cocktail
423 (BioTools, B14002) and 10 µM PMSF, and incubated for 10 min on ice. Animals were
424 lysed by TissueRuptor (Qiagen, 9001271) with Motor unit “6” for 30 sec on ice. After
425 incubation on ice for 5 minutes and centrifugation at 5,000 rpm at 4℃ for 2 min, the
426 supernatant was collected as the cytoplasmic part. The nuclear pellet was washed three
427 times with lysis buffer and resuspended in 150 µl RIPA buffer (Thermo Fisher Scientific,
428 P89900) for 30 min on ice, spun at 12,000 rpm for 15 min, and the supernatant was
429 collected as nuclear extract. Tubulin and H3 were separately used as cytoplasm and
430 nuclear loading control. For RNAi experiments, *zip-10p::zip-10::EGFP::FLAG* animals

were bleached and the eggs were laid onto RNAi plates. Animals were harvested as L4/young adults and subject to Western blot analysis as described above.

Chromatin and RNA immunoprecipitation (ChIP-QPCR and RIP-QPCR)

ChIP-QPCR assay was carried out as before with modifications. Briefly, CW-treated animals (4^{o}C for 4 hrs, recovered at 25^{o}C for 1 hr) and control (25^{o}C) animals were harvested and washed by 1 X PBS. The pellet animals were resuspended in cross-linking buffer (1% formaldehyde in 1 X PBS) followed by homogenization using TissueRuptor with Motor unit “4” for 1 min at room temperature. The process was then stopped by addition of glycine (125 mM final concentration). After washing and discarding the supernatant, the pellet was resuspended in lysis buffer and lysed by TissueRuptor with Motor unit “6” for 1 min on ice, with lysate kept on ice for additional 3 min, and then repeated 3 times. The lysate was centrifuged to collect the supernatant and one percent of the aliquot was used as “Input”. Lysate was precleared by adding salmon sperm DNA/protein-A agarose beads (Bioworld, 20182011-1), rotating at 4^{o}C for 1 hour. After centrifugation, supernatant was divided equally and added with 50 µg Flag antibody (Sigma, F3165) and mouse IgG (Santa Cruz Biotechnology, sc-2025) respectively. The samples were incubated and rotated overnight at 4^{o}C. Next, salmon sperm DNA/protein-A agarose beads were added for 2 hrs at 4^{o}C. The beads-antibody-TF-DNA complex was washed extensively and the complex and input were diluted with proteinase K buffer. The samples were then incubated at 55^{o}C for 4 hrs and then at 65^{o}C overnight to reverse crosslink. DNA was extracted by phenol-chloroform-isoamylalcohol (Sigma-Aldrich,

77617). *asp-17* promoter was measured by QPCR and calculated by the percent input method. Primers for ChIP-QPCR: *asp-17* promoter (Forward, TTCGCTGCACCTATATGTTG; Reverse, CCGCTAATACCCTTATCAC).

RNA immunoprecipitation (RIP)-QPCR assay was carried out as before with modifications to accommodate our reagents (Kershner and Kimble, 2010). Briefly, synchronous day-1 *isy-1p::isy-1::mcherry* animals were divided into two groups. One group is control (25ºC) and the other is cold-warming (4ºC for 4 hours, recovered at 25ºC for 1 hour). Animals were harvested and washed by M9 buffer until the supernatant was clear, and then washed once in buffer A and twice in lysis buffer. About 250 µl worm pellets were frozen in liquid nitrogen twice and homogenized using TissueRuptor with Motor unit “4” for 1 min on ice. The lysate was kept on ice for 15 min and centrifuged to collect the supernatant and 1% of the aliquot was kept as “Input”. Equal amount of supernatant was added with RFP-Trap®_MA (Chromotek) and rotated for 4 hrs at 4ºC. IP magnetic agarose beads were washed and 10% of IP beads were boiled for 6 min in 2X Laemmli Sample Buffer. RNA was eluted from remaining beads using 200 µl lysis buffer of Quick-RNA MiniPrepkit (Zymo Research, R1055) and extracted following the instruction. RNA was quantified with a Nanodrop device. 500 ng RNA was reverse transcribed into cDNA and Qpcr was performed as before. Relative mRNA was calculated by THE percent input method. Primers for RIP-qPCR: Primary *mir-60* Forward TCGAAAACCGCTTGTTCTTG, Reverse CGATTTCTCAAGTCTTGAACTAG; *cebp-1* Forward GATCCTTCGCAAGACAAGAC, Reverse CACATTGTCGGTAGGAACGTC.

475 Cold tolerance assay

476 Animals were cultured under non-starved conditions for at least 4 generations at
477 25^{o}C before cold tolerance assay. For cold tolerance assay of L1-stage animals, bleach-
478 synchronized populations were kept at 4^{o}C for 96 hrs and then recovered for 4 hrs at
479 25^{o}C. For cold tolerance assay of adults, animals were raised at 25^{o}C from hatching with
480 excessive bacteria food on agar plates. Well-fed L4 stage animals were transferred to
481 new plates and kept at 25^{o}C overnight to reach day-1 adulthood. To cold shock the
482 animals, agar plates were spread with equal distance on a thin plastic board and
483 transferred to a constant 4^{o}C cold room for the indicated duration. After cold shock,
484 animals were then moved to 25^{o}C for recovery for 4 hrs before scoring survival rates.
485 Animals were scored as dead if they showed no movement upon light touch.

486

487 Imaging and fluorescence quantification

488 smFISH of *C. elegans* and imaging were performed as previously described (Ji
489 and Oudenaarden, 2005). For Nomarski and fluorescence imaging, spinning-disc
490 confocal and digital automated epifluorescence microscopes (EVOS, Life Technologies)
491 were used to capture images of animals after RNAi or CW treatments. Synchronous
492 population of worms were randomly picked and treated with 1 mM levamisole water
493 solution to paralyze the animals. The animals were mounted on an agar pad on a slide
494 and aligned for imaging. Identical conditions and settings were used for both control and
495 test groups. For quantification of fluorescence images, the animals in the images were
496 outlined and signals were quantified by ImageJ software. The intensity of an individual

497 animal was obtained by dividing the total signal by the area of that animal. The average
498 intensity of the control group was set to be 1.0, to which all other intensities were
499 normalized. Graphpad Prism software was used to plot the data.

500

501 Small RNA-seq and bioinformatics

502 For small RNA sequencing, total RNA was isolated by the Quick-RNA MiniPrep kit
503 (Zymo Research, R1055) that yields total RNA including small RNAs ranging 17-200 nt.
504 RNA samples extracted from triplicate N2 animals and *isy-1* mutants were submitted to
505 Beijing Genomics Institute for small RNA library construction and sequencing. The low-
506 quality reads were filtered and clean reads were mapped to the *C. elegans* genome using
507 Bowtie2 program (Langmead and Salzberg, 2012). MiRDeep2 (Friedländer et al., 2012)
508 was used to characterize known and predict novel miRNAs. The small RNA expression
509 level was calculated as TPM (transcript per million). Differentially expressed small RNAs
510 were detected by DESeq2 (Love et al., 2014). The threshold for differentially expressed
511 sRNAs was adjusted P-value ≤ 0.05 and the absolute value of Log2ratio ≥ 1. Targets of
512 miRNAs were predicted by TargetScan (Jan et al., 2011), RNAhybrid (Krüger and
513 Rehmsmeier, 2006) and miRanda (John et al., 2004) using default parameters.

514

515 Statistical analysis

516 Data were analyzed using GraphPad Prism Software (Graphpad, San Diego, CA) and
517 presented as means ± S.D. unless otherwise specified with p values calculated by

unpaired Student's t-tests, one-way or two-way ANOVA (comparisons across more than two groups) and adjusted with Bonferroni's corrections.

Acknowledgements

We thank the *Caenorhabditis* Genetics Center, National BioResource Project in Japan and the Million Mutation Project for *C. elegans* strains. The work was supported by NIH grants R01GM117461, R00HL116654, ADA grant 1-16-IBS-197, Pew Scholar Award, Alfred P. Sloan Foundation Fellowship, and Packard Fellowship in Science and Engineering (D.K.M), R01AG032435 (Y.W.) and a CPSF postdoctoral fellowship (W.J.).

References

Al-Fageeh, M.B., and Smales, C.M. (2006). Control and regulation of the cellular responses to cold shock: the responses in yeast and mammalian systems. Biochem. J. *397*, 247–259.

Bailey, T.L., Boden, M., Buske, F.A., Frith, M., Grant, C.E., Clementi, L., Ren, J., Li, W.W., and Noble, W.S. (2009). MEME SUITE: tools for motif discovery and searching. Nucleic Acids Res. *37*, W202-208.

Baird, N.A., Douglas, P.M., Simic, M.S., Grant, A.R., Moresco, J.J., Wolff, S.C., Yates, J.R., Manning, G., and Dillin, A. (2014). HSF-1-mediated cytoskeletal integrity determines thermotolerance and life span. Science *346*, 360–363.

Bautista, D.M. (2015). Spicy science: David Julius and the discovery of temperature-sensitive TRP channels. Temp. Austin Tex *2*, 135–141.

Bindea, G., Mlecnik, B., Hackl, H., Charoentong, P., Tosolini, M., Kirilovsky, A., Fridman, W.-H., Pagès, F., Trajanoski, Z., and Galon, J. (2009). ClueGO: a Cytoscape plug-in to decipher functionally grouped gene ontology and pathway annotation networks. Bioinforma. Oxf. Engl. *25*, 1091–1093.

Brenner, S. (1974). The genetics of Caenorhabditis elegans. Genetics *77*, 71–94.

544 Brunquell, J., Morris, S., Lu, Y., Cheng, F., and Westerheide, S.D. (2016). The genome-wide
545 role of HSF-1 in the regulation of gene expression in Caenorhabditis elegans. BMC Genomics
546 *17*.

547 Choi, H.A., Badjatia, N., and Mayer, S.A. (2012). Hypothermia for acute brain injury--
548 mechanisms and practical aspects. Nat. Rev. Neurol. *8*, 214–222.

549 Chüeh, A.C., Tse, J.W., Dickinson, M., Ioannidis, P., Jenkins, L., Tögel, L., Tan, B., Luk, I.,
550 Dávalos-Salas, M., Nightingale, R., et al. (2017). ATF3 repression of BCL-XL determines
551 apoptotic sensitivity to HDAC inhibitors across tumour types. Clin. Cancer Res.
552 clincanres.0466.2017.

553 Davis, M.W., Hammarlund, M., Harrach, T., Hullett, P., Olsen, S., and Jorgensen, E.M. (2005).
554 Rapid single nucleotide polymorphism mapping in C. elegans. BMC Genomics *6*, 118.

555 Dempersmier, J., Sambeat, A., Gulyaeva, O., Paul, S.M., Hudak, C.S.S., Raposo, H.F., Kwan,
556 H.-Y., Kang, C., Wong, R.H.F., and Sul, H.S. (2015). Cold-inducible Zfp516 activates UCP1
557 transcription to promote browning of white fat and development of brown fat. Mol. Cell *57*, 235–
558 246.

559 Dix, I., Russell, C., Yehuda, S.B., Kupiec, M., and Beggs, J.D. (1999). The identification and
560 characterization of a novel splicing protein, Isy1p, of Saccharomyces cerevisiae. RNA N. Y. N *5*,
561 360–368.

562 Du, P., Wang, L., Sliz, P., and Gregory, R.I. (2015). A Biogenesis Step Upstream of
563 Microprocessor Controls miR-17∼92 Expression. Cell *162*, 885–899.

564 Fan, W., and Evans, R.M. (2015). Turning up the heat on membrane fluidity. Cell *161*, 962–963.

565 Friedländer, M.R., Mackowiak, S.D., Li, N., Chen, W., and Rajewsky, N. (2012). miRDeep2
566 accurately identifies known and hundreds of novel microRNA genes in seven animal clades.
567 Nucleic Acids Res. *40*, 37–52.

568 Frøkjaer-Jensen, C., Davis, M.W., Hopkins, C.E., Newman, B.J., Thummel, J.M., Olesen, S.-P.,
569 Grunnet, M., and Jorgensen, E.M. (2008). Single-copy insertion of transgenes in Caenorhabditis
570 elegans. Nat. Genet. *40*, 1375–1383.

571 Galej, W.P., Wilkinson, M.E., Fica, S.M., Oubridge, C., Newman, A.J., and Nagai, K. (2016).
572 Cryo-EM structure of the spliceosome immediately after branching. Nature *537*, 197–201.

573 Garrity, P.A., Goodman, M.B., Samuel, A.D., and Sengupta, P. (2010). Running hot and cold:
574 behavioral strategies, neural circuits, and the molecular machinery for thermotaxis in C. elegans
575 and Drosophila. Genes Dev. *24*, 2365–2382.

576 Giuliodori, A.M., Di Pietro, F., Marzi, S., Masquida, B., Wagner, R., Romby, P., Gualerzi, C.O.,
577 and Pon, C.L. (2010). The cspA mRNA is a thermosensor that modulates translation of the cold-
578 shock protein CspA. Mol. Cell *37*, 21–33.

579 Gomez-Pastor, R., Burchfiel, E.T., and Thiele, D.J. (2017). Regulation of heat shock
580 transcription factors and their roles in physiology and disease. Nat. Rev. Mol. Cell Biol.

Hamilton, W.D. (1963). The Evolution of Altruistic Behavior. Am. Nat. *97*, 354–356.

Hartman, M.G., Lu, D., Kim, M.-L., Kociba, G.J., Shukri, T., Buteau, J., Wang, X., Frankel, W.L., Guttridge, D., Prentki, M., et al. (2004). Role for Activating Transcription Factor 3 in Stress-Induced β-Cell Apoptosis. Mol. Cell. Biol. *24*, 5721–5732.

Hwang, A.B., and Lee, S.-J. (2011). Regulation of life span by mitochondrial respiration: the HIF-1 and ROS connection. Aging *3*, 304–310.

Jan, C.H., Friedman, R.C., Ruby, J.G., and Bartel, D.P. (2011). Formation, regulation and evolution of Caenorhabditis elegans 3'UTRs. Nature *469*, 97–101.

Ji, N., and Oudenaarden, A. van (2005). Single molecule fluorescent in situ hybridization (smFISH) of C. elegans worms and embryos (WormBook).

John, B., Enright, A.J., Aravin, A., Tuschl, T., Sander, C., and Marks, D.S. (2004). Human MicroRNA targets. PLoS Biol. *2*, e363.

Kamath, R.S., and Ahringer, J. (2003). Genome-wide RNAi screening in Caenorhabditis elegans. Methods San Diego Calif *30*, 313–321.

Kandror, O., Bretschneider, N., Kreydin, E., Cavalieri, D., and Goldberg, A.L. (2004). Yeast adapt to near-freezing temperatures by STRE/Msn2,4-dependent induction of trehalose synthesis and certain molecular chaperones. Mol. Cell *13*, 771–781.

Kato, M., Kashem, M.A., and Cheng, C. (2016). An intestinal microRNA modulates the homeostatic adaptation to chronic oxidative stress in C. elegans. Aging *8*, 1979–2005.

Kershner, A.M., and Kimble, J. (2010). Genome-wide analysis of mRNA targets for Caenorhabditis elegans FBF, a conserved stem cell regulator. Proc. Natl. Acad. Sci. U. S. A. *107*, 3936–3941.

Kim, D., Langmead, B., and Salzberg, S.L. (2015). HISAT: a fast spliced aligner with low memory requirements. Nat. Methods *12*, 357–360.

Krüger, J., and Rehmsmeier, M. (2006). RNAhybrid: microRNA target prediction easy, fast and flexible. Nucleic Acids Res. *34*, W451-454.

Kumsta, C., Chang, J.T., Schmalz, J., and Hansen, M. (2017). Hormetic heat stress and HSF-1 induce autophagy to improve survival and proteostasis in C. elegans. Nat. Commun. *8*, 14337.

Landis, J.N., and Murphy, C.T. (2010). Integration of diverse inputs in the regulation of Caenorhabditis elegans DAF-16/FOXO. Dev. Dyn. Off. Publ. Am. Assoc. Anat. *239*, 1405–1412.

Langmead, B., and Salzberg, S.L. (2012). Fast gapped-read alignment with Bowtie 2. Nat. Methods *9*, 357–359.

Liao, Y., Smyth, G.K., and Shi, W. (2014). featureCounts: an efficient general purpose program for assigning sequence reads to genomic features. Bioinforma. Oxf. Engl. *30*, 923–930.

Longo, V.D., Mitteldorf, J., and Skulachev, V.P. (2005). Programmed and altruistic ageing. Nat. Rev. Genet. *6*, 866–872.

617 Love, M.I., Huber, W., and Anders, S. (2014). Moderated estimation of fold change and
618 dispersion for RNA-seq data with DESeq2. Genome Biol. *15*, 550.

619 Lyons, J.M., Keith, A.D., and Thomason, I.J. (1975). Temperature-induced phase transitions in
620 nematode lipids and their influence on respiration. J. Nematol. *7*, 98–104.

621 Ma, D.K., Vozdek, R., Bhatla, N., and Horvitz, H.R. (2012). CYSL-1 interacts with the O2-
622 sensing hydroxylase EGL-9 to promote H2S-modulated hypoxia-induced behavioral plasticity in
623 C. elegans. Neuron *73*, 925–940.

624 Ma, D.K., Li, Z., Lu, A.Y., Sun, F., Chen, S., Rothe, M., Menzel, R., Sun, F., and Horvitz, H.R.
625 (2015). Acyl-CoA Dehydrogenase Drives Heat Adaptation by Sequestering Fatty Acids. Cell
626 *161*, 1152–1163.

627 Maere, S., Heymans, K., and Kuiper, M. (2005). BiNGO: a Cytoscape plugin to assess
628 overrepresentation of gene ontology categories in biological networks. Bioinforma. Oxf. Engl.
629 *21*, 3448–3449.

630 Mahat, D.B., Salamanca, H.H., Duarte, F.M., Danko, C.G., and Lis, J.T. (2016). Mammalian
631 Heat Shock Response and Mechanisms Underlying Its Genome-wide Transcriptional
632 Regulation. Mol. Cell *62*, 63–78.

633 Mello, C.C., Kramer, J.M., Stinchcomb, D., and Ambros, V. (1991). Efficient gene transfer in
634 C.elegans: extrachromosomal maintenance and integration of transforming sequences. EMBO
635 J. *10*, 3959–3970.

636 Metzstein, M.M., Stanfield, G.M., and Horvitz, H.R. (1998). Genetics of programmed cell death
637 in C. elegans: past, present and future. Trends Genet. TIG *14*, 410–416.

638 Morrison, S.F. (2016). Central control of body temperature. F1000Research *5*.

639 Murray, P., Hayward, S.A.L., Govan, G.G., Gracey, A.Y., and Cossins, A.R. (2007). An explicit
640 test of the phospholipid saturation hypothesis of acquired cold tolerance in Caenorhabditis
641 elegans. Proc. Natl. Acad. Sci. U. S. A. *104*, 5489–5494.

642 Ohta, A., Ujisawa, T., Sonoda, S., and Kuhara, A. (2014). Light and pheromone-sensing
643 neurons regulates cold habituation through insulin signalling in *Caenorhabditis elegans*. Nat.
644 Commun. *5*, ncomms5412.

645 Peng, Y., Zhang, M., Zheng, L., Liang, Q., Li, H., Chen, J.-T., Guo, H., Yoshina, S., Chen, Y.-Z.,
646 Zhao, X., et al. (2017). Cysteine protease cathepsin B mediates radiation-induced bystander
647 effects. Nature *547*, 458–462.

648 Peter, M.E. (2011). Programmed cell death: Apoptosis meets necrosis. Nature *471*, 310–312.

649 Polderman, K.H. (2009). Mechanisms of action, physiological effects, and complications of
650 hypothermia. Crit. Care Med. *37*, S186-202.

651 Ritchie, A., Gutierrez, O., and Fernandez-Luna, J.L. (2009). PAR bZIP-bik is a novel
652 transcriptional pathway that mediates oxidative stress-induced apoptosis in fibroblasts. Cell
653 Death Differ. *16*, 838–846.

654 Sapolsky, R.M. (2004). Why Zebras Don't Get Ulcers, Third Edition (New York: Holt
655 Paperbacks).

656 Schmieder, R., and Edwards, R. (2011). Quality control and preprocessing of metagenomic
657 datasets. Bioinforma. Oxf. Engl. *27*, 863–864.

658 Skulachev, V.P. (1999). Phenoptosis: programmed death of an organism. Biochem. Biokhimiia
659 *64*, 1418–1426.

660 Skulachev, V.P. (2002). Programmed death phenomena: from organelle to organism. Ann. N. Y.
661 Acad. Sci. *959*, 214–237.

662 Smith, J.M. (1964). Group Selection and Kin Selection. Nature *201*, 1145–1147.

663 Solís, E.J., Pandey, J.P., Zheng, X., Jin, D.X., Gupta, P.B., Airoldi, E.M., Pincus, D., and Denic,
664 V. (2016). Defining the Essential Function of Yeast Hsf1 Reveals a Compact Transcriptional
665 Program for Maintaining Eukaryotic Proteostasis. Mol. Cell *63*, 60–71.

666 Tansey, E.A., and Johnson, C.D. (2015). Recent advances in thermoregulation. Adv. Physiol.
667 Educ. *39*, 139–148.

668 Thorvaldsdóttir, H., Robinson, J.T., and Mesirov, J.P. (2013). Integrative Genomics Viewer
669 (IGV): high-performance genomics data visualization and exploration. Brief. Bioinform. *14*, 178–
670 192.

671 Vriens, J., Nilius, B., and Voets, T. (2014). Peripheral thermosensation in mammals. Nat. Rev.
672 Neurosci. *15*, 573–589.

673 Yenari, M.A., and Han, H.S. (2012). Neuroprotective mechanisms of hypothermia in brain
674 ischaemia. Nat. Rev. Neurosci. *13*, 267–278.

675 Yura, T., Nagai, H., and Mori, H. (1993). Regulation of the heat-shock response in bacteria.
676 Annu. Rev. Microbiol. *47*, 321–350.

677 Zhou, X., Feng, X., Mao, H., Li, M., Xu, F., Hu, K., and Guang, S. (2017). RdRP-synthesized
678 antisense ribosomal siRNAs silence pre-rRNA via the nuclear RNAi pathway. Nat. Struct. Mol.
679 Biol. *24*, 258–269.

680 Zhu, J.-K. (2016). Abiotic Stress Signaling and Responses in Plants. Cell *167*, 313–324.

681

682 **Figure legends**

683 **Figure 1: *asp-17* is robustly and specifically induced by cold-warming. A**, Volcano

684 plot of RNA-seq showing differentially regulated genes (up-regulated genes in red;

685 down-regulated genes in green; *asp-17* was indicated by purple dot) by cold-warming in

686 wild type *C. elegans*. **B**, RNA-seq reads at the *asp-17* locus showing consistent up-
687 regulation of *asp-17* transcript levels in triplicate samples after cold-warming. **C**, QPCR
688 measurements of gene expression levels showing up-regulation of three representative
689 CW inducible genes, including *asp-17*, after shifting from 25^{o}C to different degrees of
690 hypothermia (4, 10, 15 and 22^{o}C) lasting 2 hrs followed by recovery at 25^{o}C for 0.5 hr.
691 **D**, Quantification of RNA-seq reads indicating specific up-regulation of *asp-17* but not
692 other members of the *asp* family genes (only expressed *asp* genes are shown). **E**,
693 QPCR measurements of *asp-17* levels under conditions of indicated durations of cold
694 and warming (with or without 25^{o}C recovery for “yes/no”). **F**, smFISH images showing
695 *asp-17* up-regulation (signals indicated by yellow) by CW predominantly in the intestine
696 of wild type but not *asp-17* null animals. n ≥ 20 total animals for each group with N ≥ 3
697 independent biological replicates; *** indicates P < 0.001. Scale bar: 50 μm.

698

699 **Figure 2: A forward genetic screen identifies *C. elegans isy-1* as a causal**
700 **regulator of *asp-17*::GFP expression. A**, Schematic of the *C. elegans* ISY-1 protein
701 showing the domain structure predicted by SMART (top) (http://smart.embl-
702 heidelberg.de) and a multiple sequence alignment of ISY-1 homologues from major
703 metazoans showing the conservation of the glutamate residue substituted to lysine by
704 the *dma50* mutation isolated from EMS screens. **B**, Nomarski and fluorescence images
705 showing the phenotype of intestinal *asp-17p*::GFP in wild type and *dma50* mutants. **C**,
706 Fluorescence images showing the distribution of ISY-1::GFP driven by the endogenous
707 *isy-1* promoter. Arrows indicate neuronal, hypodermal and intestinal nuclei. **D**, Nomarski
708 and fluorescence images showing intestinal *asp-17p*::GFP in a transgenic strain

expressing RNAi against *isy-1* specifically in intestine. **E**, Schematic of the *C. elegans* *isy-1* gene with mCherry tagged at the C-terminus (top); Nomarski and fluorescence images showing rescue of *dma50* by various transgenes (below). **F,** Quantification of fluorescence intensities showing rescue of *dma50* in *asp-17p*::GFP activation. N ≥ 3 independent biological replicates; *** indicates P < 0.001. Scale bar: 20 μm.

Figure 3: ZIP-10 acts downstream of ISY-1 and mediates transcriptional response to CW. A, QPCR measurements of *asp-17* levels induced by CW in wild type and *isy-1(dma50)* mutants. **B**, Volcano plot of RNA-seq showing differentially regulated genes (up-regulated genes in red; down-regulated genes in green) in *isy-1* mutants compared with wild type. **C**, RNA-seq measurements of expression levels for indicated genes in wild type and *isy-1(dma50)* mutants. **D**, Nomarski and fluorescence images showing *asp-17p*::*GFP* induction by *isy-1* RNAi was blocked in *zip-10* mutants. **E**, Western blots of the integrated *zip-10p*::*zip-10*::*EGFP::FLAG* strain showing time-dependent protein induction by CW. **F**, Western blots of the integrated *zip-10p::zip-10::EGFP::FLAG* strain showing its up-regulation by *isy-1* RNAi and down-regulation by *GFP* or *zip-10* RNAi. Both short- and long-exposure blots are shown. **G**, Western blots of the integrated *zip-10p::zip-10::EGFP::FLAG* strain showing its up-regulation strictly required warming after cold shock. **H**, Western blots of the integrated *zip-10*p::*zip-10::EGFP::FLAG* strain showing its up-regulation by CW was further enhanced by *isy-1* RNAi. **I**, QPCR measurements of gene expression levels showing ZIP-10 dependent up-regulation of *asp-17* and *cpr-3* but not *srr-6* or *F53B9.1* after cold for indicated durations and 1-hr

731 warming. n ≥ 20 total animals for each group with N ≥ 3 independent biological
732 replicates; *** indicates P < 0.001. Scale bar: 20 µm.

733

734 **Figure 4: ISY-1 regulates *zip-10* via *mir-60*. A,** Western blot of mCherry/RFP-trapped
735 RNA immunoprecipitates in animals treated with or without cold-warming. **B,** QPCR
736 measurements of the percent input for primary *mir-60* transcripts from mCherry/RFP-
737 trapped RNA immunoprecipitates in animals treated with or without cold-warming. **C,**
738 QPCR measurements of the percent input for *cbp-1* transcripts from mCherry/RFP-
739 trapped RNA immunoprecipitates in animals treated with or without cold-warming. **D,**
740 QPCR measurements of the mature *mir-60* transcript levels from wild type, *isy-*
741 *1(dma50)* and *mir-60(n4947)* deletion mutants. **E,** QPCR measurements of the levels of
742 CW-inducible gene transcripts in animals with indicated genotypes and conditions. **F,**
743 Western blot of lysates from animals carrying the array *ges-1p::mCherry::3'utr(zip-10)*
744 reporters with CW or *isy-1* RNAi. No change of reporter activity was observed. **G,**
745 Western blot of lysates from animals carrying *zip-10p::zip-10::EGFP::FLAG* reporters
746 with various indicated CW and RNAi conditions. n ≥ 20 total animals for each group with
747 N ≥ 3 independent biological replicates; *** indicates P < 0.001; ** indicates P < 0.01.

748

749 **Figure 5: ISY-1 and ZIP-10 regulate a genetic program to promote organismic**
750 **death. A,** Venn diagram indicating numbers of genes commonly regulated by CW and
751 *isy-1(dma50)* mutants. **B**, Scatter plot depicting the correlation between the
752 transcriptome response to cold (y-axis) and the transcriptome response to *isy-1*

753 mutation (x-axis). Shown are the log2 fold changes compared with corresponding
754 controls. Pearson correlation coefficient and the associated P-value were calculated
755 using R functions. **C**, AT-rich motif identified by MEME enriched among the CW and *isy-*
756 *1(dma50)* regulated genes, with a table listing numbers of the motif present in top-
757 ranked 4 genes. **D**, ChIP-QPCR measurements of ZIP-10::FLAG binding to the *asp-17*
758 promoter. **E**, Survival rates of indicated genotypes after prolonged CW (4^{o}C for 48 hrs
759 followed by 4 hrs of warming). **F**, Organismic death rates of indicated genotypes after
760 heat shock (32^{o}C) induction of *zip-10* wild type, mutant with defective transactivation C-
761 terminus, *zip-2* and *zip-11* (left), without CW. Nomarski image (right) indicate
762 morphologies of normal and dead animals with induction of *zip-10*. **G**, RNA-seq
763 measurements of gene targets of indicated TFs. **H**, Table showing the *asp-17p::GFP*
764 and cold tolerance phenotypes of animals with indicated genotypes. **I**, Model for the role
765 and regulation of the ZIP-10 pathway. n ≥ 20 total animals for each group with N ≥ 3
766 independent biological replicates; *** indicates P < 0.001.

767

768 **Figure 1-figure supplement 1: RNA-seq identified genes up-regulated by cold-**
769 **warming. A**, Hierarchical clustering analysis of genes up- and down-regulated genes by
770 CW. **B**, Gene ontology analysis of genes up- and down-regulated genes by CW.

771

772 **Figure 2-figure supplement 1: EMS screens identified *isy-1* as a regulator of *asp-***
773 ***17*. A**, Fluorescence images showing up-regulation of *asp-17p::GFP* but not the co-
774 injection marker *unc-54p::mCherry* by CW. **B**, Schematic illustrating the workflow of

775 EMS mutagenesis to isolate mutants with abnormal *asp-17p::GFP* expression. **C**, Table
776 showing the mutants isolated from the screen, including *dma50* that defines the gene
777 *F53B7.3*, named as *isy-1*. **D**, Chromosome genetic maps showing DraI SNP sites and
778 the mapped interval for *dma50*. **E**, Table listing candidate genes with mutations
779 identified by WGS, with two genes highlighted in yellow within the mapped interval. **F**,
780 fluorescence images showing that RNAi of *isy-1* phenocopies *dma50*. N ≥ 3
781 independent biological replicates; *** indicates P < 0.001. Scale bar: 20 μm.

782

783 **Figure 2-figure supplement 2: ISY-1 is a *C. elegans* member of evolutionarily**
784 **conserved protein family and its level is not regulated by cold-warming. A,**
785 Multiple sequence alignment (Cluster Omega, visualized by Jalview) of ISY-1 family
786 members in major metazoan species. **B**, Cladogram of ISY family proteins. **C**, Sanger
787 sequencing confirmation of *isy-1(dma50)*. **D,** RNA-seq measurements of *isy-1* and *asp-*
788 *17* levels under CW conditions and in *isy-1(dma50)* mutants. **E**, Western blot of *isy-*
789 *1*p::ISY-1::mCherry showing no regulation by CW. N ≥ 3 independent biological
790 replicates; *** indicates P < 0.001.

791

792 **Figure 3-figure supplement 1: ISY-1 does not affect general splicing of a GFP**
793 **reporter nor specific splicing of *zip-10*. A**, Nomarski and fluorescence images
794 showing that animals with *isy-1* RNAi are not defective in general intron splicing of an
795 *eft-3p::GFP* (intron-containing) reporter. **B**, Read plot from RNA-seq of wild type at the
796 *zip-10* locus. **C**, Read plot from RNA-seq of *isy-1(dma50)* mutants at the *zip-10* locus

797 indicating the intact splicing of the *zip-10* intron despite increased mRNA levels. **D,**
798 Normalized QPCR measurements of mRNA expression levels of *isy-1* and *zip-10* from
799 wild type and *isy-1(dma50)* mutants. **E,** Normalized QPCR measurements of mRNA
800 expression levels of *isy-1* and *zip-10* from wild type and CW-treated animals.

801

802 **Figure 3-figure supplement 2: Mechanisms of regulation and function of *zip-10*. A**,
803 Nomarski and fluorescence images showing the *zip-10p::GFP* reporter activated by *isy-*
804 *1* RNAi. **B**, Western blot of lysates from *zip-10p::zip-10::EGFP::FLAG* transgenic
805 animals showing its increased abundance after CW but not by hypoxia (0.5% O_2) or
806 starvation for 24 hrs. **C**, Western blot of fractionated lysates from *zip-10p::zip-*
807 *10::EGFP::FLAG* transgenic animals after CW showing its increased abundance in
808 cytosol and nucleus. **D**, Western blot of lysates from *zip-10p::zip-10::EGFP::FLAG*
809 transgenic animals showing its increased abundance after CW when warming was
810 permitted and cold exposure was prolonged. **E**, Western blot of lysates from *zip-*
811 *10p::zip-10::FLAG* transgenic and various RNAi treated animals showing its increased
812 abundance after CW in *isy-1* RNAi treated animals but was unaffected by RNAi against
813 *C37C3.2*, encoding the *C. elegans* orthologue of translation initiation factor 5 (eIF5), or
814 *T26A8.4*, encoding the *C. elegans* orthologue of *Saccharomyces cerevisiae* Caf120, a
815 component of the Ccr4-Not deadenylase RNA-degrading complex. **F**, ZIP-10 domain
816 organization based on analysis by SMART (smart.embl-heidelberg.de) and modeled
817 structure of ZIP-10's bZIP domain (swissmodel.expasy.org). **G**, Sequence alignment of
818 ZIP-10's bZIP domain and the Maf transcription factor as a template of the modelled
819 ZIP-10 structure. **H**, Schematic of the *zip-10* locus showing the wild type, EGFP::FLAG

820 tagged allele, and the wild-type and C-terminal transactivation mutant ZIP-10 protein
821 sequences. The mutated residues (from Q and N to V and A, respectively) at the ZIP-10
822 C-terminus are completely conserved in nematodes.

823

824 **Figure 4-figure supplement 1: A specific subset of CW-inducible genes is**
825 **dependent on ZIP-10.** Shown is a table of fold induction for gene expression levels
826 determined by QPCR measurements of top-ranked randomly selected CW-inducible
827 genes in wild type and *zip-10* mutant animals.

828

829 **Figure 5-figure supplement 1: Identification of differentially regulated microRNAs**
830 **in wild type and *isy-1(dma50)* mutants. A,** Summary table showing the read statistics
831 for the small RNA-seq experiments using three biologically triplicate samples in wild
832 type and *isy-1(dma50)* mutants**. B**, Small RNA length distribution plots for wild type and
833 *isy-1(dma50)* mutants. **C**, Distribution graphs for various types of small RNAs identified
834 by small RNA sequencing for wild type and *isy-1(dma50)* mutants. **D**, Volcano plot
835 showing the differentially regulated microRNAs, including *mir-60*, in the *isy-1(dma50)*
836 mutants (three replicates each). **E**, Schematic of two examples illustrating the TF-
837 encoding genes, *skn-1* and *daf-16* at 3' UTRs, targeted by two microRNAs, *mir-51* and
838 *mir-359*, respectively, which are down-regulated in *isy-1(dma50)* mutants. **F**,
839 Hierarchical clustering analysis of microRNAs up- or down-regulated in *isy-1(dma50)*
840 mutants. *mir-51* and *mir-359* down-regulation were indicated by arrows.

841

Figure 5-figure supplement 2: ZIP-10 constitutes a genetic program promoting kin selection of *C. elegans* under resource-limiting and stress conditions. A, Mathematical model illustrating the advantage of wild-type (red line) versus *zip-10* KO animals (blue line) at the population level under growth resource-liming and thermal stress conditions. Individual fitness distribution (x-axis) after cold-warming thermal stress is set to be exponential (thin red line) and linear (thin blue line) to fit the phenotypic differences in death rates of wild type and *zip-10* KO animals and to simplify comparison and calculation. Given the same period of time and the same amount of growth resources (integral differences between thin and thick lines), wild-type population yields more thermal stress-adapted reproducing animals than *zip-10* deficient animals. The parameters for integrals were adjusted so that the "growth resources" are the same despite that the population growth modes are different for wild type and *zip-10* KO. **B**, Schematic illustrating an exemplar situation of the mathematical model in which 5 post-reproduction adults and 5 larvae are living in a food-limiting condition. After cold-warming thermal stress, wild-type adults die out, leaving food for young larvae to grow into reproductive adults whereas *zip-10* KO post-reproduction adults do not die, consuming the limited food and competing out the young larvae so that fewer reproductively active *zip-10* KO animals emerge from such conditions. **C**, Experimental evidence indicating the specific induction of *zip-10p::zip-10::EGFP::FLAG* by CW as measured by Western blot in adults but not in larvae. **D**, Survival rates of wild type and *zip-10* KO (*ok3462*) animals at different stages after prolonged CW thermal stresses (96-hr cold shock for L1 while 48-hr for others) showing that ZIP-10's pro-death

effects are more prominent in old animals. n ≥ 20 total animals for each group with N ≥ 3 independent biological replicates; *** indicates P < 0.001, ** indicates P < 0.01.

Figure 1-source data 1: Lists of genes up- and down-regulated by CW with adjusted P < 0.05 and log2FoldChange from biological triplicate samples of wild-type *C. elegans*.

Figure 3-source data 1: Lists of genes up- and down-regulated by the *isy-1(dma50)* mutation with adjusted P < 0.05 and log2FoldChange from biological triplicate samples of wild-type and *isy-1(dma50)* mutant *C. elegans*.

Figure 5-source data 1: Lists of genes commonly regulated by CW and the *isy-1(dma50)* mutation with adjusted P < 0.05 and log2FoldChange from biological triplicate samples of wild-type and *isy-1(dma50)* mutant *C. elegans*.

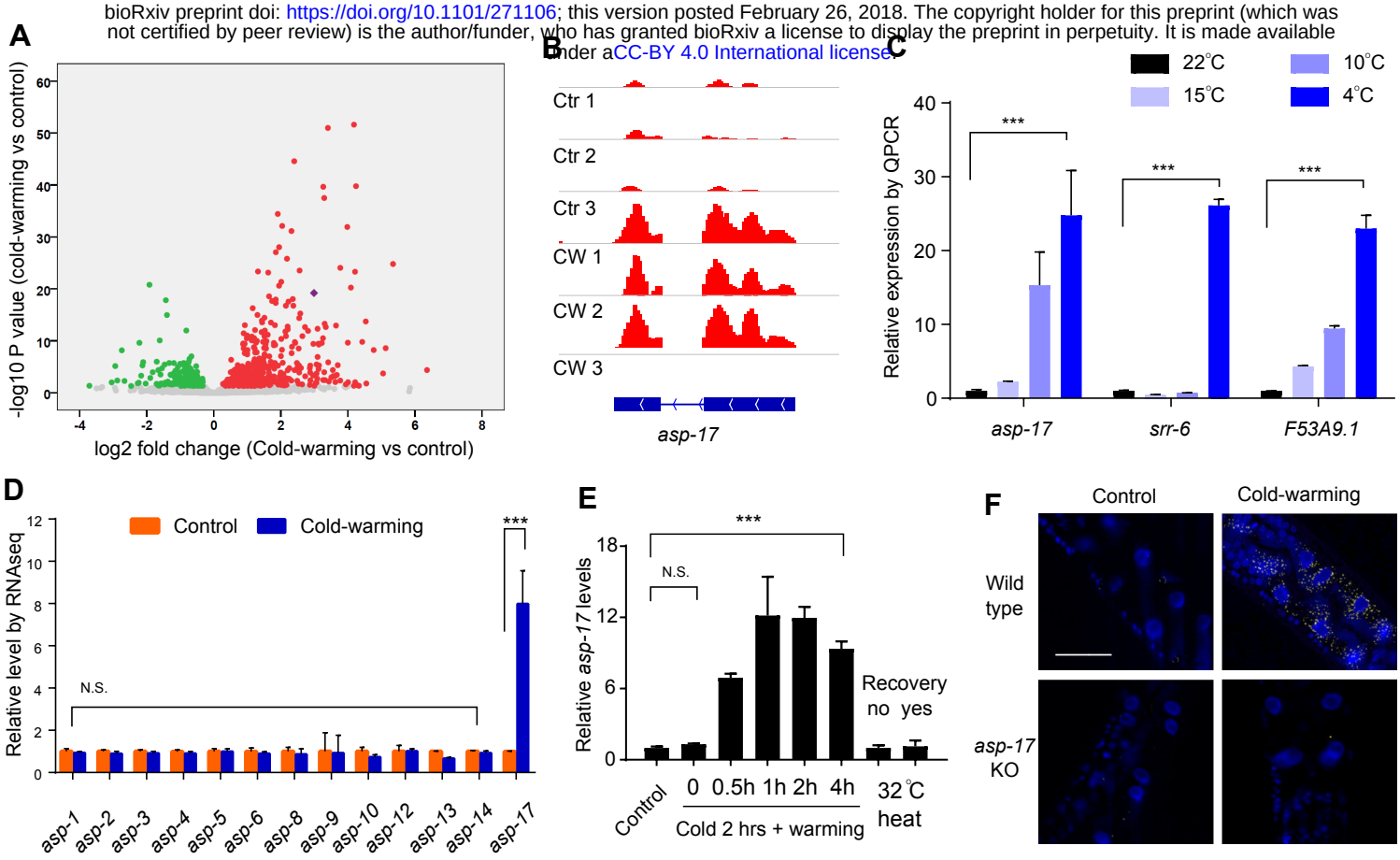

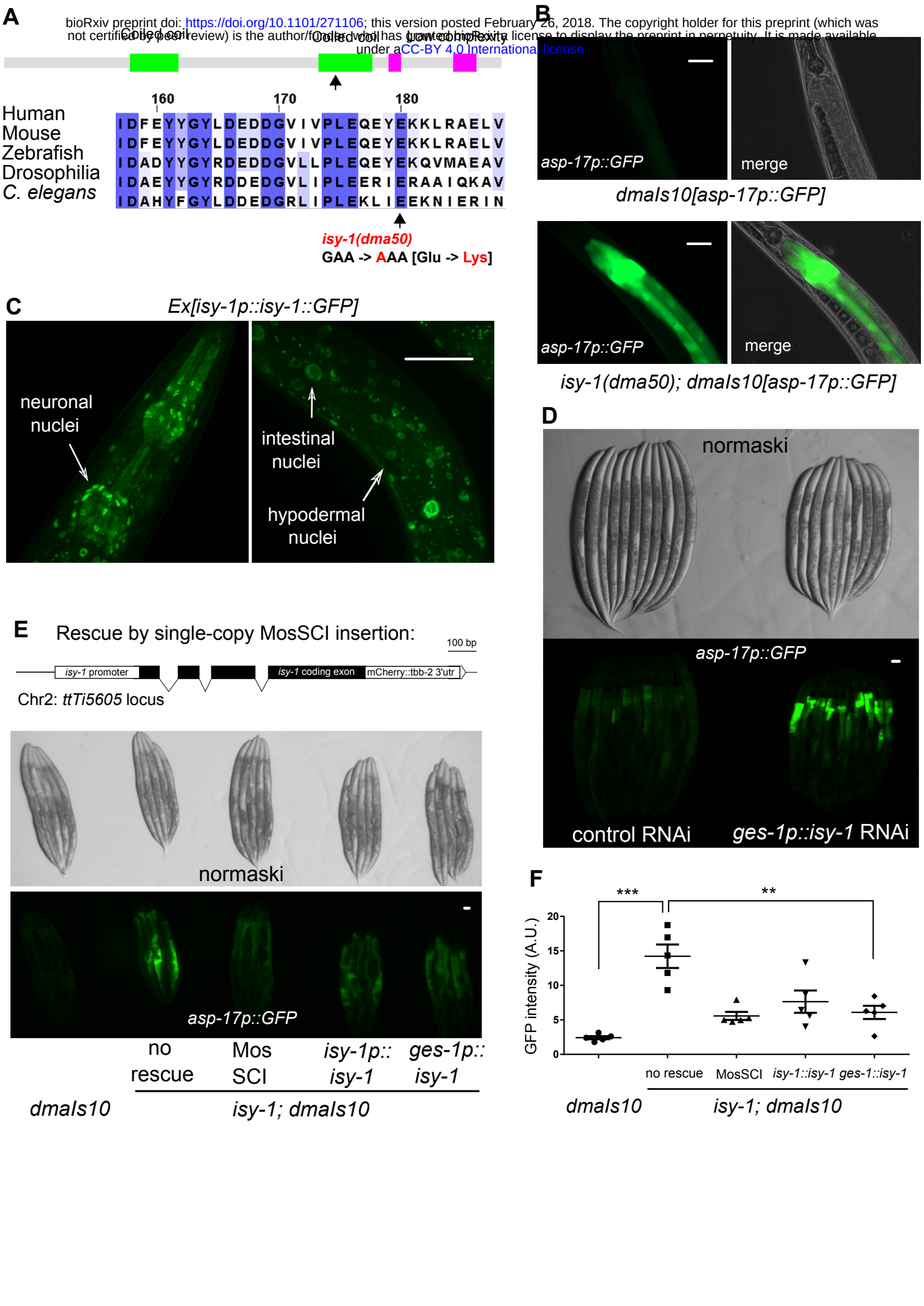

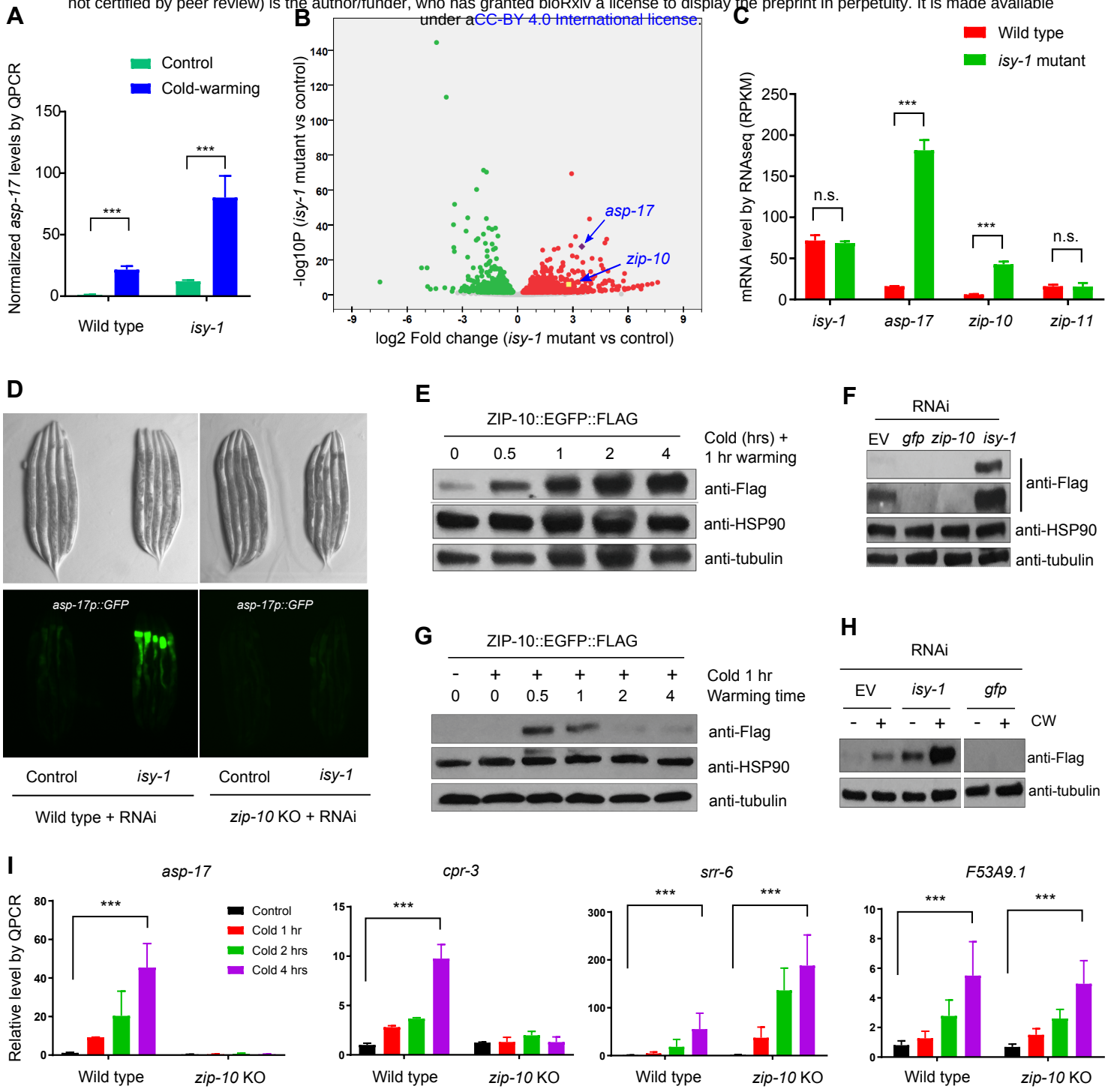

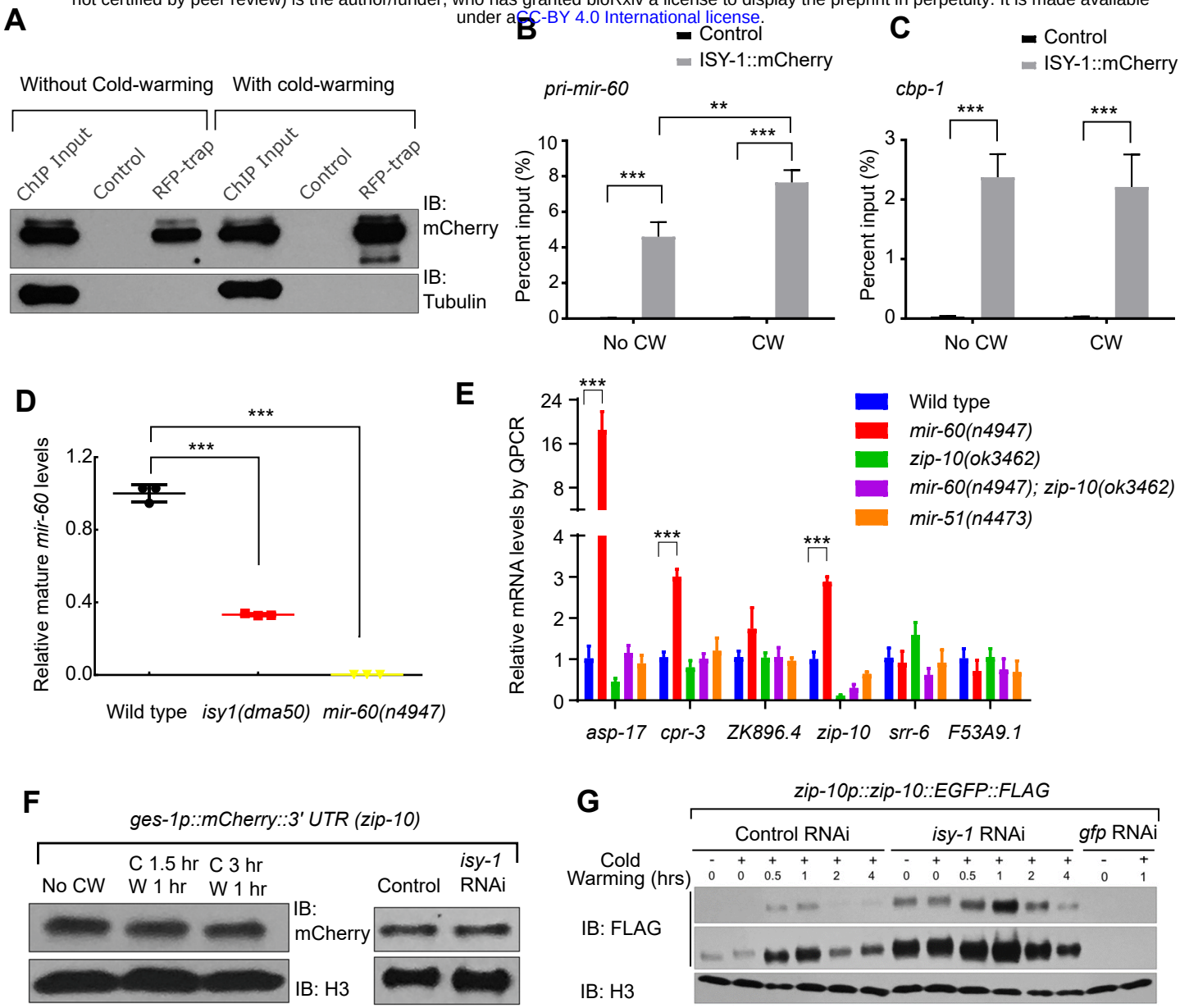

A

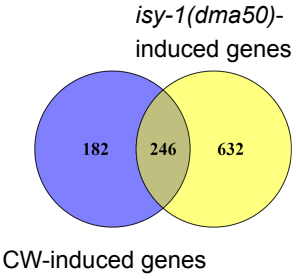

B

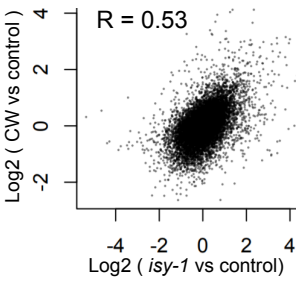

C

Numbers of motifs	
asp-17p	16
F08G2.5p	5
clec-66p	2
M02H5.8p	1

D

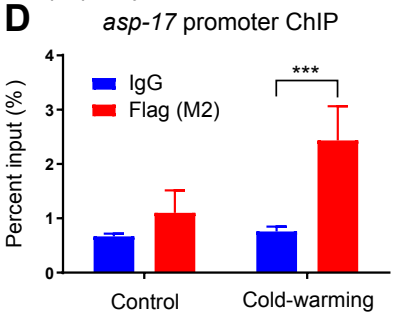

E

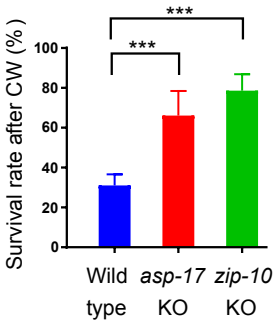

F

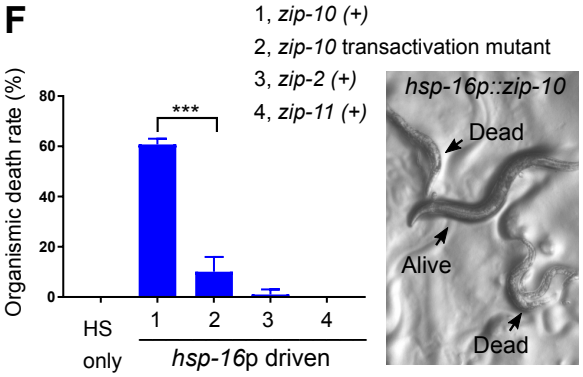

G

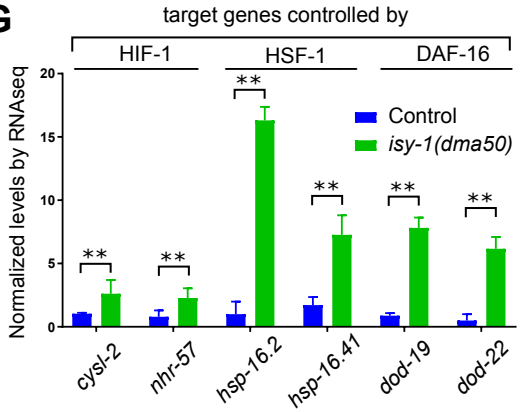

H

Genotype	*asp-17p*::GFP	Cold tolerance (n > 100)
Wild type	+	32%
isy-1(dma50) or isy-1 RNAi	+++++	57%
zip-10(ok3462); isy-1 RNAi	+	82%
zip-10(ok3462)	+	78%
mir-60(n4947)	++++	29%
mir-60(n4947); zip-10(ok3462)	+	51%
asp-17(dma99)	+	68%
asp-17(dma99); isy-1 RNAi	+++++	72%
daf-16(mu86)	+	10%
daf-16(mu86); isy-1 RNAi	+++++	38%

I

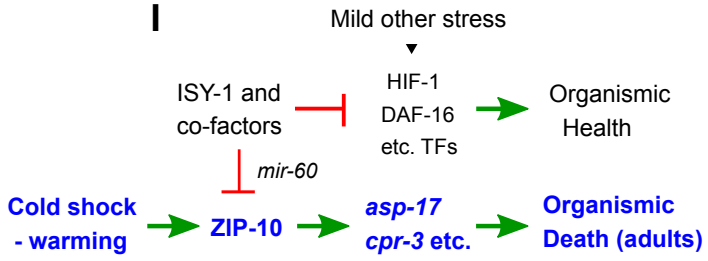

A

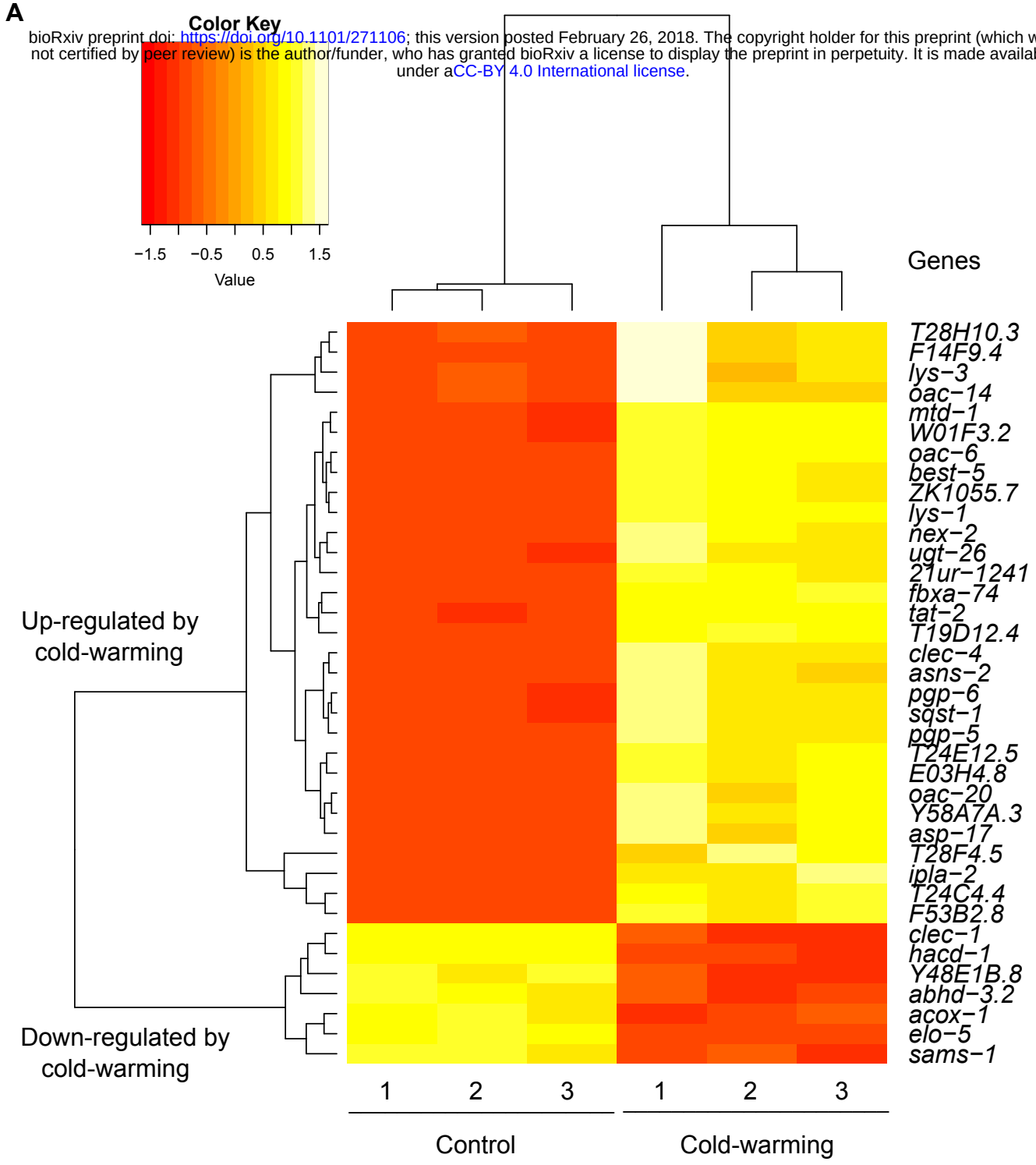

B

GOID	GOTerm	Term P-Value
KEGG:00071	Fatty acid degradation	0.068035515
KEGG:00330	Arginine and proline metabolism	0.012703481
KEGG:00564	Glycerophospholipid metabolism	0.027845609
KEGG:02010	ABC transporters	6.87E-07
KEGG:04068	FoxO signaling pathway	0.099454727
KEGG:04136	Autophagy	0.010025137
KEGG:04137	Mitophagy	0.002142392
KEGG:04140	Autophagy	0.007908727
KEGG:04141	Protein processing in endoplasmic reticulum	0.129746247
KEGG:04144	Endocytosis	0.005199927
KEGG:04310	Wnt signaling pathway	0.050156699
KEGG:04350	TGF-beta signaling pathway	0.034403422

Figure 2-figure supplement 1

A

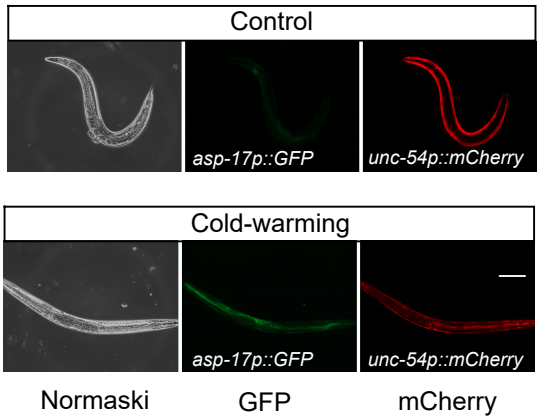

B

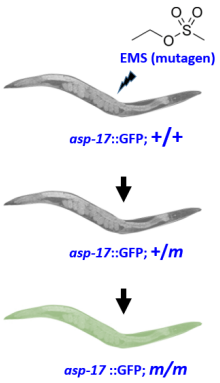

C

Genotype	Chr.	*asp-17*::GFP	Mutation	HomoloGene
Wild type		+		
dma37, dma38, dma70, dma72	I	++++		
dma60, dma62	IV	+++		
dma50	V	+++++	*F53B7.3*	***ISY1***
dma65, dma68, dma69, dma66	V	+++++		
dma76	X	+++		

D

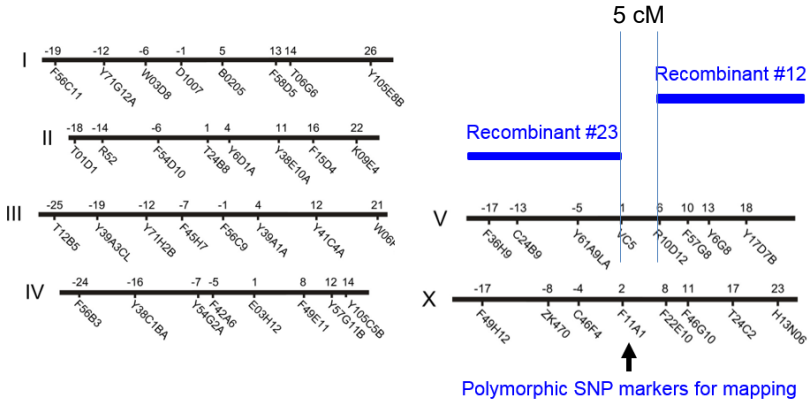

E

ID	Chr	Position	Type	Mutation	Gene
137831	V	5755472	missense	CAT->CCT[His->Pro]	{K09H11.11}
137833	V	5755482	missense	CAG->AAG[Gln->Lys]	{K09H11.11}
137834	V	5755509	missense	CAG->AAG[Gln->Lys]	{K09H11.11}
137835	V	5755526	missense	AAA->ACA[Lys->Thr]	{K09H11.11}
137836	V	5755527	missense	AAA->CAA[Lys->Gln]	{K09H11.11}
138694	V	6176589	missense	GTC->TTC[Val->Phe]	{W06H8.8}
138696	V	6177078	missense	CCA->GCA[Pro->Ala]	{W06H8.8}
138723	V	6182672	missense	CAA->CCA[Gln->Pro]	{W06H8.8}
144570	V	9229947	missense	GAT->GAG[Asp->Glu]	{F07C3.3}
144573	V	9229951	missense	ATT->AGT[Ile->Ser]	{F07C3.3}
145051	V	9472465	missense	AGT->AGA[Ser->Arg]	{F07D3.2}
145605	V	9775413	missense	GGT->GAT[Gly->Asp]	{F46B6.12}
147935	V	10999964	missense	GAA->AAA[Glu->Lys]	{F53B7.3}
149300	V	11729925	missense	ATG->TTG[Met->Leu]	{B0240.1}
150620	V	12432165	missense	TTC->ATC[Phe->Ile]	{C54D10.13}
150754	V	12491030	missense	GTT->TTT[Val->Phe]	{W04D2.3}
153483	V	13948723	missense	TAT->GAT[Tyr->Asp]	{R10D12.5}
154125	V	14265193	missense	CCT->TCT[Pro->Ser]	{F40G12.3}
154807	V	14585363	missense	CAA->CTA[Gln->Leu]	{Y40H4A.2}
154808	V	14585364	missense	CAA->GAA[Gln->Glu]	{Y40H4A.2}
156519	V	15432409	missense	GAG->GAT[Glu->Asp]	{T26H5.8}
164074	V	19037276	missense	CTC->CAC[Leu->His]	{Y39B6A.24}
164075	V	19037278	missense	CAT->CAG[His->Gln]	{Y39B6A.24}
164076	V	19037279	missense	CAT->CTT[His->Leu]	{Y39B6A.24}
164077	V	19037280	missense	CAT->TAT[His->Tyr]	{Y39B6A.24}

F

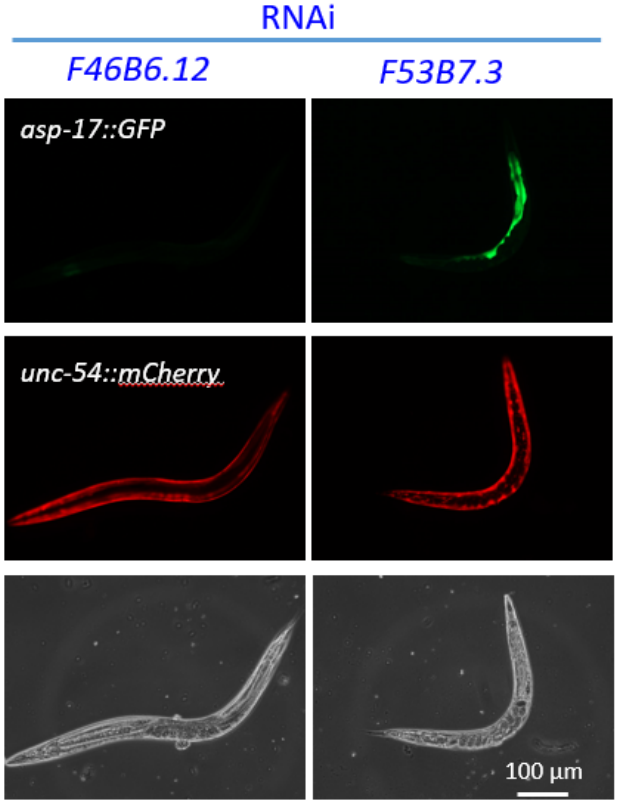

Figure 2-figure supplement 2

A

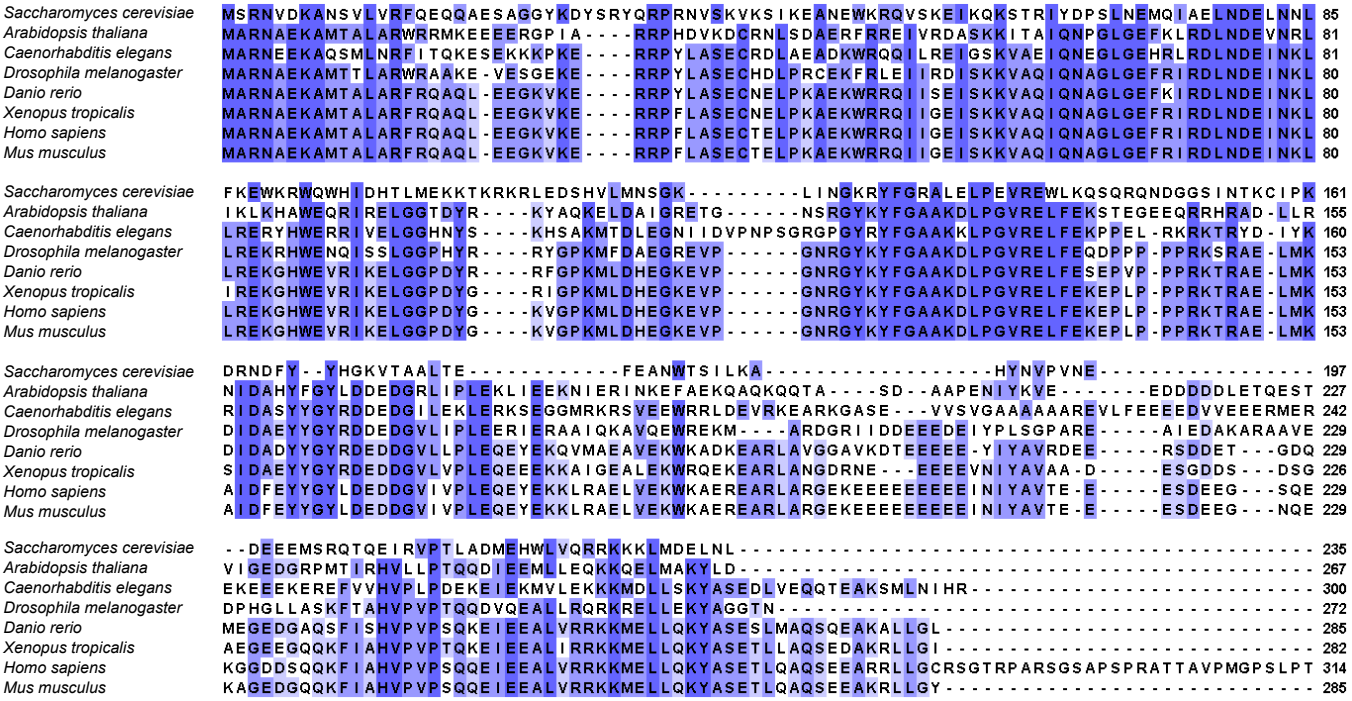

B

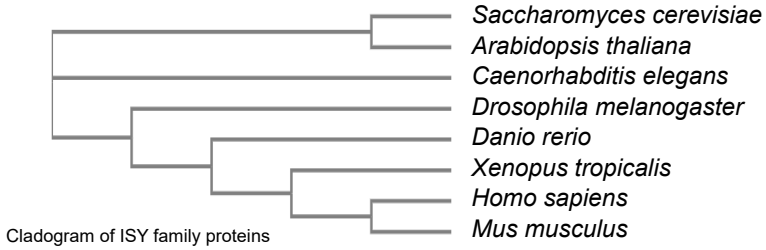

C

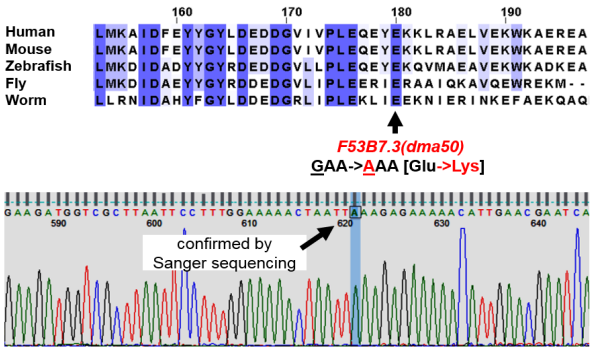

D

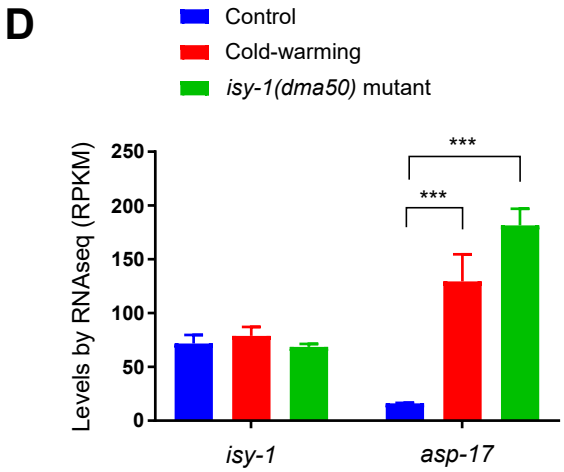

E

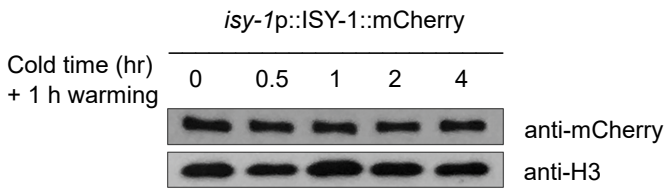

Figure 3-figure supplement 1

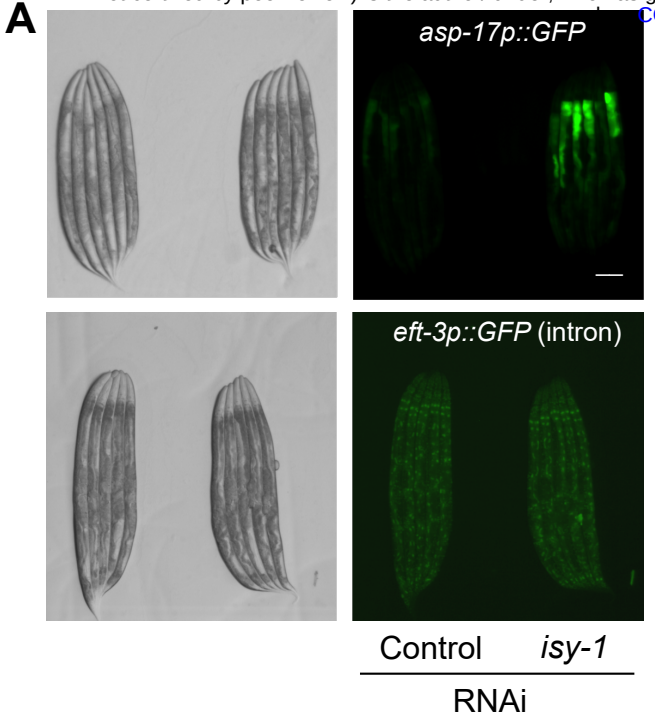

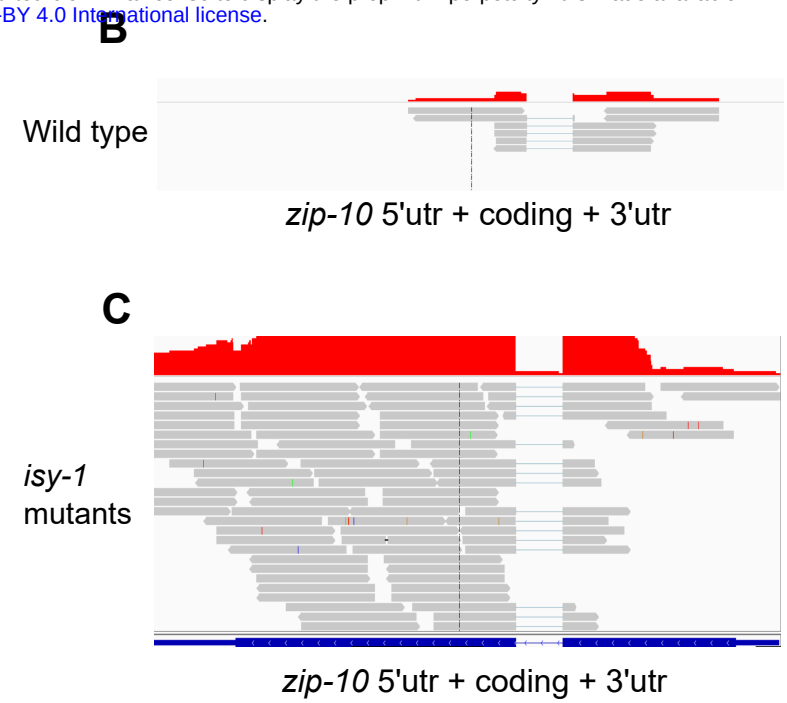

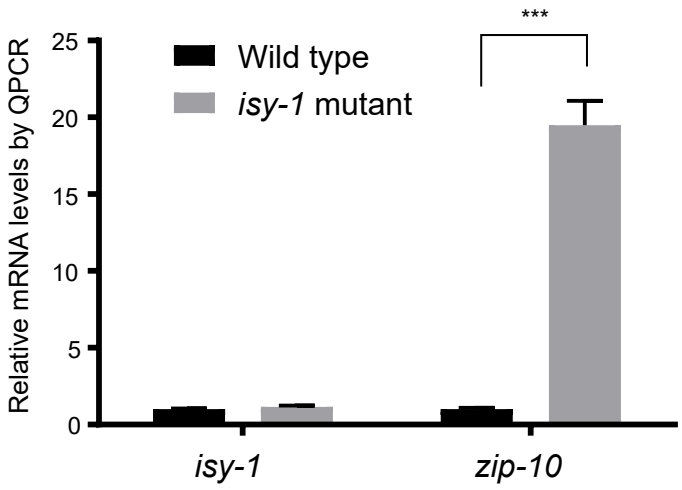

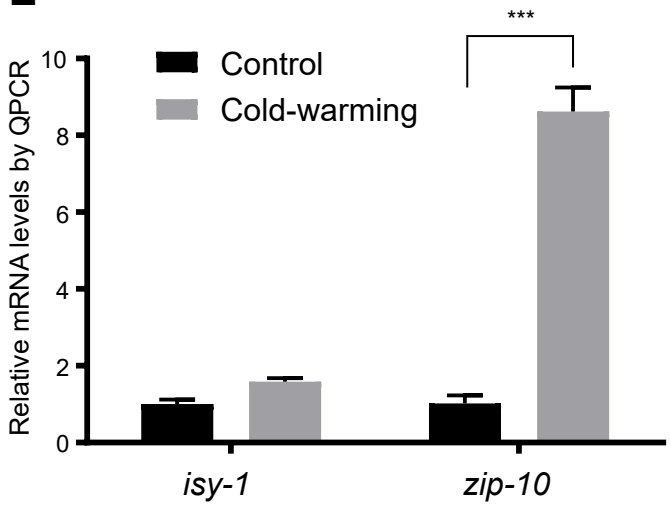

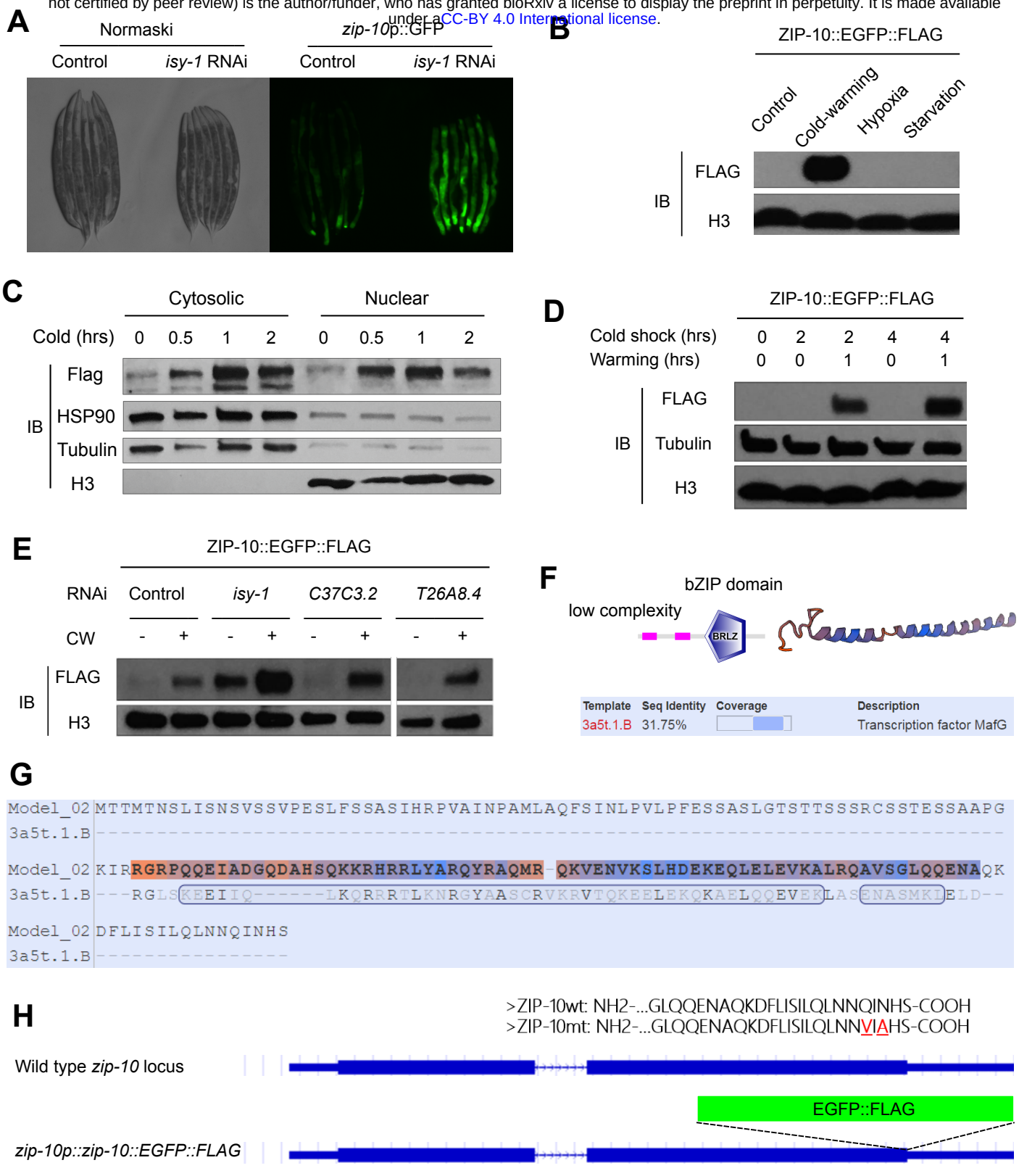

Figure 4-Figure Supplement 1: Relative mRNA levels of CW-inducible genes in wild-type and *zip-10* mutants.

Gene		1	2	3	4	*P* value
asp-17	WT	1.20±0.22	9.20±0.07	20.38±12.77	45.45±12.47	
	zip-10 m	0.37±0.04	0.46±0.12	0.71±0.29	0.43±0.10	0.025
cpr-3	WT	1.01±0.18	2.80±0.16	3.67±0.10	9.75±1.43	
	zip-10 m	1.24±0.05	1.31±0.48	1.99±0.40	1.30±0.52	0.005
ZK896.4	WT	1.01±0.20	3.56±1.27	6.31±1.13	12.22±2.00	
	zip-10 m	1.19±0.07	0.76±0.07	1.14±0.07	1.03±0.21	0.009
F53A9.1	WT	0.80±0.29	1.27±0.48	2.78±1.07	5.51±2.29	
	zip-10 m	0.69±0.19	1.50±0.42	2.60±0.62	4.95±1.56	0.748
srr-6	WT	1.09±0.29	4.68±2.84	18.31±15.68	55.37±33.32	
	zip-10 m	1.74±0.53	37.31±22.32	136.49±46.46	188.14±64.10	0.050
ceh-37	WT	1.04±0.35	1.75±0.15	2.36±0.56	5.52±1.12	
	zip-10 m	0.76±0.40	1.76±0.65	2.58±0.57	3.53±0.59	0. 072
fis-2	WT	1.09±0.57	0.94±0.36	2.92±0.09	8.57±2.12	
	zip-10 m	2.19±0.47	3.55±0.44	4.57±0.24	11.93±1.98	0. 115
CYP14A5	WT	0.98±0.14	2.53±0.46	7.54±2.90	26.04±5.55	
	zip-10 m	3.99±1.29	6.77±0.77	10.12±0.78	28.57±5.66	0. 610
sqst-1	WT	0.98±0.29	2.59±1.15	4.95±1.08	13.59±4.28	
	zip-10 m	2.68±0.54	5.81±0.25	8.13±0.59	12.85±2.95	0. 820
best-5	WT	0.97±0.31	1.79±0.40	5.34±3.24	18.21±6.83	
	zip-10 m	1.37±0.97	2.94±0.26	6.06±2.23	13.35±4.41	0. 368
tsp-1	WT	1.05±0.41	6.78±2.86	18.03±6.33	72.47±13.72	
	zip-10 m	3.04±2.34	12.53±4.52	23.45±2.73	50.02±9.17	0. 108
dod-3	WT	1.08±0.54	9.42±4.50	18.04±2.08	33.69±6.53	
	zip-10 m	2.64±1.17	8.11±2.47	13.19±3.75	28.77±6.74	0. 415
oac-20	WT	1.00±0.09	4.19±0.56	7.92±0.49	19.54±3.53	
	zip-10 m	1.38±0.08	2.90±1.17	5.05±1.01	16.20±4.87	0. 396
F37C4.5	WT	1.01±0.17	2.10±0.38	2.79±1.84	8.94±2.34	
	zip-10 m	1.43±0.18	1.49±0.27	2.19±0.33	5.28±1.69	0. 100
dod-19	WT	1.08±0.45	0.95±0.01	0.67±0.02	1.41±0.37	
	zip-10 m	1.33±0.07	0.85±0.09	0.97±0.18	1.75±0.23	0. 262
dod-22	WT	1.15±0.74	1.52±0.1.	1.27±0.22	2.76±0.50	
	zip-10 m	1.41±0.25	1.29±0.34	2.55±0.24	3.41±0.59	0. 226

oac-6	WT	1.01±0.12	3.07±0.77	5.36±1.28	10.94±3.72	
	zip-10 m	1.79±0.25	2.34±1.30	4.80±0.98	8.22±1.61	0. 336
K09D9.1	WT	1.05±0.38	1.05±0.58	4.01±2.82	24.56±3.64	
	zip-10 m	3.31±1.14	7.38±1.61	11.55±3.07	27.66±8.46	0. 605
clec-41	WT	1.08±0.49	0.83±0.38	1.37±0.17	2.31±0.54	
	zip-10 m	1.63±0.27	0.35±0.21	0.68±0.26	1.26±0.19	0. 065
F48E3.8	WT	1.17±0.72	0.87±0.42	2.07±0.97	5.30±1.14	
	zip-10 m	0.99±0.27	0.60±0.49	1.22±0.08	5.66±0.66	0. 666
cebp-1	WT	1.04±0.34	1.44±0.22	2.84±0.34	6.80±3.05	
	zip-10 m	2.21±0.69	2.07±0.37	3.01±0.14	4.58±0.90	0. 335

WT: wild type;
zip-10 m: *zip-10* mutant (*ok3462*);
1. 25^0C;
2. 4^0C-1h, 25^0C-1h;
3. 4^0C-2h, 25^0C-1h;
4. 4^0C-4h, 25^0C-1h.
n=3 biological replicates.

Figure 5-figure supplement 1

A

Sample name	N2_1	N2_2	N2_3	isy-1_1	isy-1_2	isy-1_3
Total read count	22976625	23109312	22295824	22444321	22245873	24302500
Clean read count	21468703	21558728	20485338	21588236	20650793	23394939
% Clean read	93.44	93.29	91.88	96.19	92.83	96.27
Mapped read count	15710018	13611645	14405480	5817319	6311661	7921648
% Mapped reads	73.18	63.14	70.32	26.95	30.56	33.86

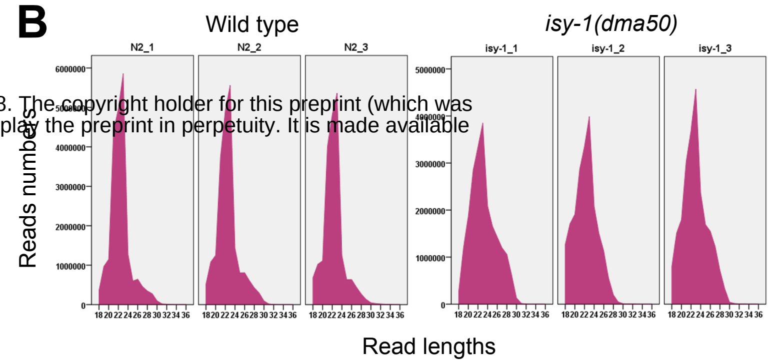

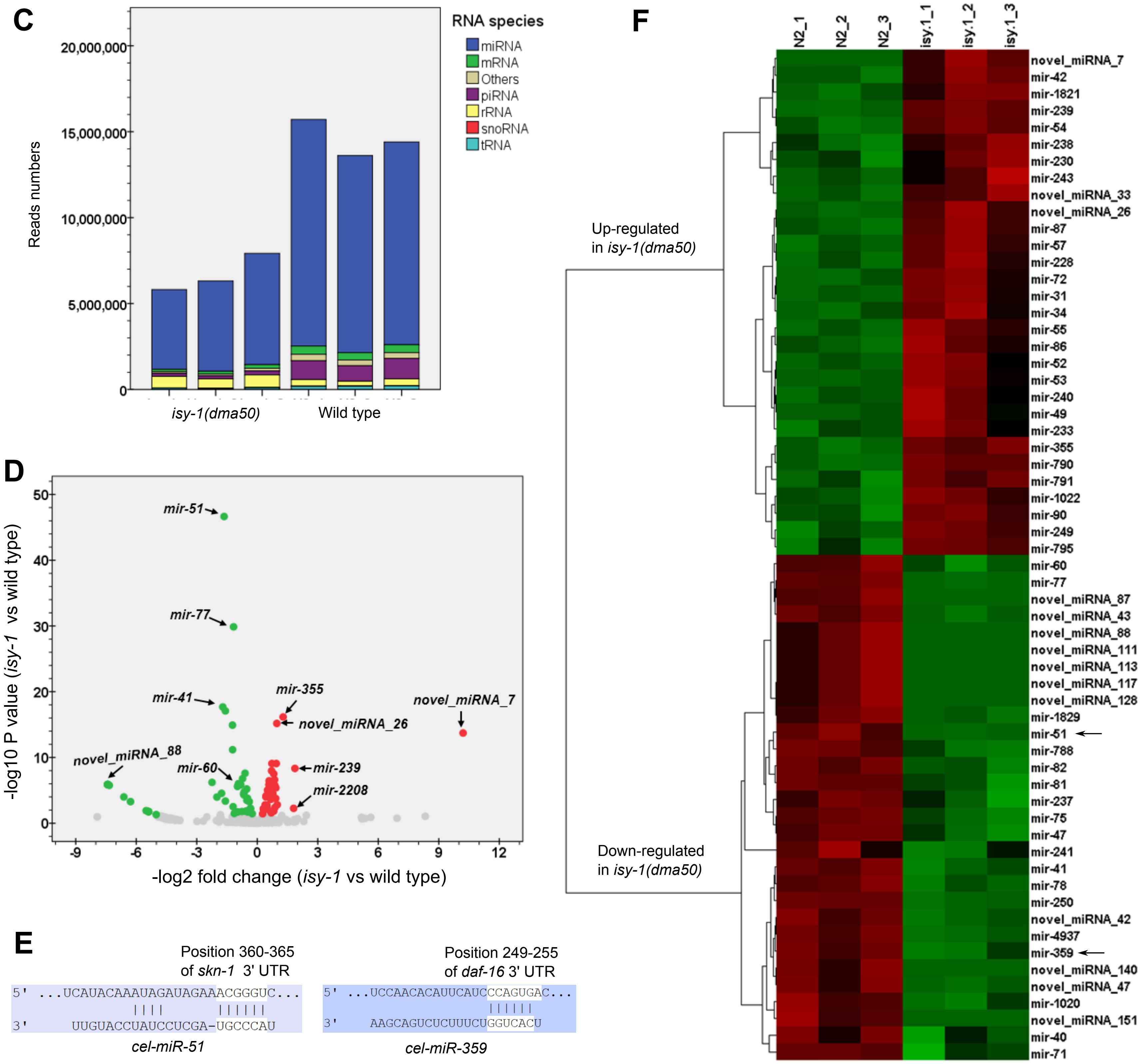

Figure 5-figure supplement 2

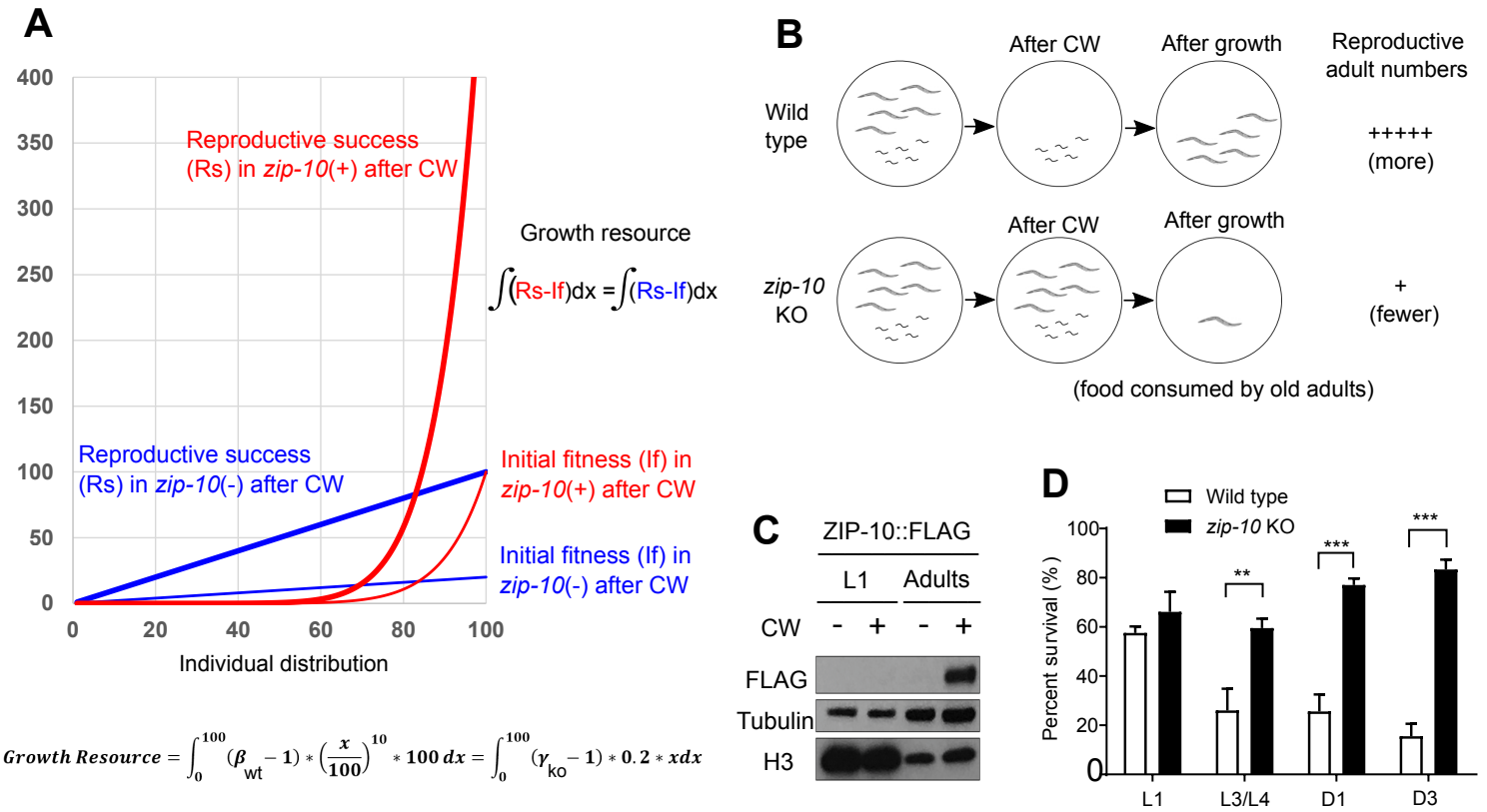

$$Growth\ Resource = \int_0^{100} (\beta_{wt} - 1) * \left(\frac{x}{100}\right)^{10} * 100\,dx = \int_0^{100} (\gamma_{ko} - 1) * 0.2 * x dx$$